

**POLITECNICO DI TORINO**

Department of Mechanical & Aerospace Engineering



- Master of Science Thesis -

**EXPERIMENTAL STUDY OF GASOLINE  
DIRECT INJECTION UNDER SPRAY  
COLLAPSE CONDITIONS**

*Supervisors:*

Dario Pastrone

Raul Payri

Abián Bautista Rodríguez

*Candidate:*

Daniele Arduino

Academic Year 2019 - 2020

EXPERIMENTAL STUDY OF GASOLINE  
DIRECT INJECTION UNDER SPRAY  
COLLAPSE CONDITIONS

Daniele Arduino

Academic Year 2019-2020





# Acknowledgments

For helping this all come together over the past five years there are many people I wish to thank and for many reasons. First of all, I would like to sincerely thank Professor Dario Pastrone (Politecnico di Torino), who initially gave me the possibility to work on such an interesting project. In addition, I am truly grateful to Raul Payri and Abián Bautista Rodríguez (CMT) for their guidance and their encouragement throughout the last semester in Valencia.

I owe a debt of gratitude to all my friends over the four past years at Politecnico di Torino, who encouraged me especially at the beginning of my career. As citing them all might take too long, I just would like to mention Dario Coluzzi, whose dedication and meticulousness have been inspirational to me. I wish to express my gratitude to all the incredible people from around the world whom I had the luck to know throughout my period abroad in Valencia. The skills I gained, the memories and friendships I made, will stay with me forever. Moreover, I could not forget to mention my friends from back home, whose early and ongoing active support means the world to me.

Most importantly, I would like to acknowledge all the members of my family, especially my parents and my siblings, along with my grandparents. They have supported me to do whatever I wanted to. I promise my time as a student is finally over, not that I'm going to bother with gimmicks like growing up just yet.

# Abstract

The pressing and unresolved issue of environmental pollution and the increasing concerns on energy supply have led to the production of vehicles with improved fuel economy and reduced emissions, becoming even more necessary. This thesis shows that the gasoline direct injection (GDI) engine will continue to develop in the coming years, becoming a key part of the automotive propulsion market.

The work presented has been carried out at CMT – *Centro Motores Térmicos*, a research centre located in Valencia, fully involved in the development of future combustion engines. The objective pursued is to analyse the behaviour of different kinds of fuel under varying operating conditions, such as temperature and pressure, of either the injected fuel or the combustion chamber.

The importance of the study regarding the spray collapse lies in the fact that this phenomenon affects the atomization of the spray, because of its impact on fuel-air mixing. Spray collapses were observed, in this work, under the elevated ambient pressure conditions, but in other investigations also under flash boiling conditions. However, it was found flash boiling may be also beneficial, since it leads to a reduction in the size of the fuel particles, with the advantage to improve the mixing between fuel and air, increasing the efficiency of the combustion and reducing pollutant emissions. Nevertheless, the effect of these phenomena on the behaviour of GDI injectors and their sprays is yet not fully understood and difficult to predict.

In the present work, experimental studies have been performed in an optically accessible constant volume vessel. The ambient pressure of the vessel ranged from 3 to 21 bar and the ambient temperature varied between 573 and 800 K. The tests have been carried out with injection pressure of 100, 200, 280 bar. High-speed imaging using DBI and the Schlieren measurement technique were utilized to investigate the spray morphology. The tested fuels were iso-octane and n-heptane. Two different kinds of fuel have been used in order to evaluate the effect of the volatility on the flash boiling process. Normal-heptane tests have been carried out mostly to compare these experiments with others in

the scientific literature.

It was observed that thermo-physical properties of the chamber are the ones that have the most significant effect on the characteristic of the spray. The results highlighted which are the determining physical quantities and how they influence the morphology of the spray.

# Contents

<b>1</b>	<b>Introduction</b>	<b>14</b>
1.1	The problem of pollutants formation . . . . .	16
1.2	State of art in various propulsion methods . . . . .	20
1.2.1	Gasoline engines . . . . .	21
1.2.2	Diesel engines . . . . .	22
1.3	Classification and properties of fuels . . . . .	22
1.3.1	Volatility . . . . .	24
1.3.2	Octane number . . . . .	26
<b>2</b>	<b>Gasoline Direct Injection Engines</b>	<b>30</b>
2.1	Introduction . . . . .	30
2.2	Operating principles . . . . .	32
2.3	Methods used for the stratification of the charge . . . . .	35
2.4	Spray injectors in GDI engines . . . . .	37
2.4.1	Pressure swirl injectors . . . . .	39
2.4.2	Multi-hole solenoid injectors . . . . .	40
2.4.3	Multi-hole piezo injectors . . . . .	41
2.5	In-cylinder charge air motion . . . . .	42
2.5.1	Squish . . . . .	44
2.5.2	Tumble . . . . .	45
2.5.3	Swirl . . . . .	46
<b>3</b>	<b>Spray Atomization</b>	<b>48</b>
3.1	Spray structure . . . . .	48
3.2	Properties influencing spray formation . . . . .	50
3.3	Disintegration process and spray break-up . . . . .	52
<b>4</b>	<b>Developments in GDI Spray Research</b>	<b>55</b>
4.1	Split injection strategies . . . . .	55
4.2	Flash boiling process . . . . .	57
4.2.1	Difference between evaporation and flash boiling . . . . .	58
4.2.2	Conditions for the flash boiling to occur . . . . .	60

4.2.3	Flash boiling mechanism: bubble nucleation and growth . . . . .	61
4.2.4	Flash Boiling in multi-hole injector sprays . . . . .	63
4.3	Spray collapse . . . . .	64
4.3.1	Jet-induced spray collapse at elevated ambient pressures . . . . .	64
4.3.2	Condensation-induced spray collapse under flash boiling conditions . . . . .	66
<b>5</b>	<b>Experimental Equipment</b>	<b>68</b>
5.1	Test rig . . . . .	68
5.2	Injection system . . . . .	70
5.3	Fuel used . . . . .	73
5.4	Optical set-up . . . . .	74
5.4.1	Single-Pass Schlieren technique . . . . .	75
5.4.2	DBI technique . . . . .	78
5.5	Test matrix . . . . .	80
<b>6</b>	<b>Experimental Techniques</b>	<b>82</b>
6.1	Introduction to the experimental strategy . . . . .	82
6.2	Image processing system . . . . .	83
6.3	Contour processing . . . . .	86
<b>7</b>	<b>Results</b>	<b>90</b>
7.1	Penetration . . . . .	90
7.1.1	Effect of gas density variation . . . . .	91
7.1.2	Effect of the injection pressure . . . . .	94
7.1.3	Effect of the type of fuel used . . . . .	96
7.1.4	Effect of the temperature chamber variation . . . . .	97
7.2	Spray angle . . . . .	99
7.2.1	Effect of injection pressure variation . . . . .	99
7.2.2	Effect of density chamber variation . . . . .	101
7.2.3	Effect of the temperature chamber variation . . . . .	104
7.2.4	Effect of the fuel type . . . . .	106
7.2.5	Effect of the injection temperature variation . . . . .	110
<b>8</b>	<b>Summary and Conclusions</b>	<b>112</b>
	<b>Bibliography</b>	<b>113</b>
	<b>Appendices</b>	<b>118</b>

# List of Figures

1.1	Trend of emissions rate in the last three decades. Note: 1990 = 100 (Source: Bruegel based on EEA)[1]	16
1.2	EU Transport greenhouse gas emissions by mode, 2015 (Source: Bruegel based on EEA)[1]	17
1.3	Trend of pollutants regulations in EU (Data Source: EEA) [3]	20
1.4	Saturation pressure curves of different kinds of fuels	24
1.5	Difference between normal combustion triggered by the spark plug (a) and detonation events (b)	27
1.6	Piston heavily damaged by detonation; at this stage, the integrity of the engine is at risk	28
2.1	Distinction between the configurations of gasoline fuelled engines: PFI (left) and GDI (right)	31
2.2	Trend of the automotive propulsion global market throughout the years	32
2.3	GDI engine operating modes	33
2.4	Schematic representation of the homogeneous mode (left) and stratified mode (right) [5]	33
2.5	Mixing stratification strategies	35
2.6	Spray from different types of GDI injector	38
2.7	Pressure swirl injector geometry of a liquid rocket engine	39
2.8	Multi-hole solenoid injector geometry	41
2.9	Internal geometry of a piezo injector	42
2.10	Phases of the turbulent flow in the combustion chamber	43
2.11	Squish generated by the shape of the cylinder head	44
2.12	Tumble	45
2.13	Swirl	47
3.1	Spray parameters	49
3.2	Correlation between break-up and surface area [14]	52
3.3	Correlation between jet break-up regimes and Ohnesorge-Reynolds break-up diagram [17]	54

4.1	Pilot and principal injection events in relation with the combustion phenomenon . . . . .	56
4.2	Saturation line of n-hexane, from [21] . . . . .	59
4.3	Stages of bubble growth [23] . . . . .	62
4.4	Different air motion between non-collapsed (left-hand side) and collapsed (right-hand side) spray . . . . .	65
4.5	Mechanisms of the condensation-induced spray collapse [25] . . . . .	66
5.1	Representation of the test rig: external side (a), upper side (b), internal side (c) [27] . . . . .	69
5.2	Opening for the resistance from the inside (a), from the outside (b) and cylinder casing of the resistance (c) . . . . .	69
5.3	Test rig arranged for the tests with screws and O-ring clearly visible . . . . .	70
5.4	External geometry of the injector (CMT) . . . . .	71
5.5	Plant of the position of orifices (left) and zooming of the nozzle tip (right) . . . . .	71
5.6	Logic control unit (left) and internal view of the test rig with the position of the injector outlined (right) . . . . .	72
5.7	Saturation curves of the tested fuels . . . . .	73
5.8	Schlieren functioning principle. From left to right: light source, indisturbed light pulses, altered path light [28] . . . . .	76
5.9	Single-mirror Schlieren setup design [29] . . . . .	77
5.10	DBI optical system setup [30] . . . . .	78
5.11	DBI equipment arranged for the tests (CMT) . . . . .	79
5.12	Focus on the light source, diffuser and lens used for the tests (CMT) . . . . .	80
6.1	Steps of the testing process . . . . .	82
6.2	Set-up of the geometry of the images . . . . .	84
6.3	Example of the image processing for a Schlieren image [26] . . . . .	85
6.4	Raw image which highlights liquid (left) and vapor (right) contour of the spray (red) and penetration (blue) . . . . .	86
6.5	Raw images in which the characterization of the liquid spray angle is marked, for different densities . . . . .	87
6.6	Raw Schlieren image . . . . .	88
7.1	Density variations for 573 K (top) and 800 K (bottom), for vapor and liquid penetration . . . . .	92

7.2	Liquid spray comparison between lower density conditions (left) and higher density conditions (right) using raw images and the detected contours . . . . .	93
7.3	Vapor spray comparison between lower density conditions (left) and higher density conditions (right) using raw images and the detected contours . . . . .	94
7.4	Injection pressure variations for iso-octane vapor and liquid penetrations . . . . .	94
7.5	Injection pressure variations for two different back temperature values: 573 K (left) and 800 K (right) . . . . .	95
7.6	Effect of fuel properties on the spray penetration, under several conditions . . . . .	96
7.7	Effect of the back temperature change on liquid and vapor penetration . . . . .	98
7.8	Effect of the injection pressure on the spray liquid angle	100
7.9	Effect of back density on spray angles at 573 K (top) and 800 K (bottom) . . . . .	101
7.10	Comparison between raw images at two different density conditions (time ASOI 1371 $\mu$ s) . . . . .	102
7.11	Density variations at non-vaporizing conditions (400 K) for liquid spray [26] . . . . .	103
7.12	Effect of the ambient temperature variation on the spray angles . . . . .	104
7.13	Combined effects of variations in ambient density and temperature for three injection pressure tested . . . . .	105
7.14	Comparison of different kinds of fuel under several conditions . . . . .	108
7.15	Saturation curve of tested fuels . . . . .	109
7.16	Comparison of raw images: iso-octane (left) and n-heptane (right) . . . . .	109
7.17	Spray morphology of iso-octane at three different fuel temperatures [33] . . . . .	110

# List of Tables

1.1	Regulations of pollutants under EU legislation [3] . . .	18
1.2	Classification of fossil fuels . . . . .	25
1.3	AKI numbers of the principal fuels . . . . .	27
2.1	Comparison of spray targeting methods . . . . .	37
4.1	Main differences between evaporation and flash boiling	58
5.1	Other specifications of the injector . . . . .	72
5.2	Test Matrix . . . . .	81
7.1	Properties of the tested fuels . . . . .	97

# Nomenclature

## Acronyms

AEOI	After End of Injection
AKI	Anti-Knock Index
ASOI	After Start of Injection
BDC	Bottom Dead Centre
CI	Compression-Ignition
CNT	Classical Nucleation Theory
DI	Direct Injection
DMI	Diffuse Back-Illumination
ECN	Engine Combustion Network
EEA	European Economic Area
EOI	End of Injection
ET	Energizing Time
GDI	Gasoline Direct Injection
ICE	Internal Combustion Engines
MON	Motor Octane Number
NIST	National Institute of Standards and Technology
PFI	Port Fuel Injection
PM	Particulate Matter
PM	Particulate Matter
PON	Pump Octane Number
POPs	Persistent Organic Pollutants
RDE	Real Driving Emissions

RdON	Road Octane Number
RON	Research Octane Number
SCH	Schlieren
SI	Spark-Ignition
SOI	Start of Injection
TDC	Top Dead Centre
TEL	Tetra-Ethyl Lead
THC	Total Hydrocarbons

## Symbols

$\rho$	Fluid Density
$\sigma$	Surface Tension
$\mu$	Dynamic Viscosity
Da	Damköhler Number
Oh	Ohnesorge Number
Re	Reynolds Number
We	Weber Number
wt%	Percentage by weight

# Chapter 1

## Introduction

Engines have evolved greatly over the course of the last few decades. Nowadays, there are a very large number of vehicle propulsion methods available and there have been many changes in the development of this technology. Forty years ago, the interest in spray technology was almost non-existent. However, the knowledge of spray generation has now become a subject of particular relevance in a wide range of applications. For instance, international congresses regarding atomization and sprays are currently held in Europe, Asia and America. The most significant example of spray application is represented by the injection of liquid fuel to generate the necessary mechanical power in cars, planes and other combustion-based vehicles. Nevertheless, liquid fuel combustion is responsible for the emission of pollutants.

With continual growth in the production of automobiles, the impact of emissions is a great threat to the environment. As a result of this atmospheric pollution, a global warming has been observed with scientists predicting future major climatic changes. To face this critical problem, in automotive design, current trends are geared towards vehicles with increased economy and reduced exhaust emissions. To control the environmental impact, regulatory bodies around the world have introduced tight and more stringent regulations.

Respecting such restrictive decisions requires both the development of new types of clean fuels and the improvement of energy efficiency in the combustion process. Moreover, the increasing price of fuel is an additional motivation for improving combustion energy efficiency.

The topic of liquid fuels is more attractive to face than that of gaseous fuels, because they are characterized by more energy per unit volume and they are easier to transport and manipulate. Due to their advantages, worldwide use of liquid fuels is not likely to be reduced anytime soon. It is for all of these reasons that, in the last decades, the interest in spray technology has become widespread throughout the world.

The availability of high-performance calculation tools, such as *Computational Fluid Dynamics* (CFD), allows a qualitative leap in terms of product development efficiency. Being a method that uses numerical analysis and algorithms to solve and analyse fluid dynamics problems, CFD allows the comparison among more solutions at reduced costs and in less time than those necessary for experimentation. However, this does not mean that experimentation loses meaning. Each mathematical model capable of simulating a physical phenomenon, in fact, requires starting data. In addition to this, the importance of experimental tests is not limited to providing the starting points but is also used to validate the calculation. For this reason, understanding which parameters control fuel vaporization and how is essential, both for the design of the engine and for the development of multidimensional models. The present investigation offers an accurate and deep understanding on the physical processes that occur in the atomization of evaporating sprays produced by gasoline direct injection.

The first section of this chapter will highlight the issue of global pollution, which represents the underlying problem to

be faced by research and development. The second part will introduce the current status and prospect of the most common propulsion methods for passenger vehicles. The third one will focus on the main properties of the fuels and their components, considering their importance for the purpose of the thesis.

### 1.1 The problem of pollutants formation

Transport delivers many benefits to our society. It allows the movement of people and good, it supports economic growth, it provides employment but, on the other hand, it is the major contributor to emissions of air pollutants in Europe, as it is clearly represented in *Figure 1.1*. Indeed, the transport sector has not seen the same gradual decline in greenhouse emissions as other sectors: emissions only started to decrease in 2007 and, at least until 2015, they remained higher than in 1990 [1].

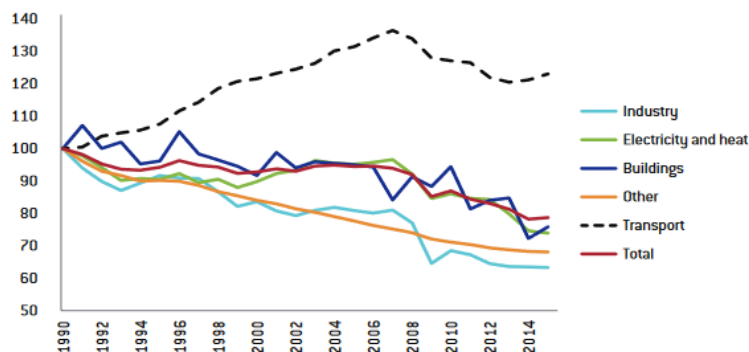


*Figure 1.1:* Trend of emissions rate in the last three decades.  
 Note: 1990 = 100 (Source: Bruegel based on EEA)[1]

Air pollution can be defined as the presence of pollutants in the atmosphere at levels that harm human health, the en-

vironment itself and the cultural heritage. Mostly since the peak of contamination of 2007, air pollution has become a problem of primary importance and has led the European Union to the development of a long-term vision to reduce greenhouse gas emissions. Policy was primarily leaning towards the sector of road transport, which is responsible for more than 70 percent of the EU transport sector’s emissions (*Figure 1.2*). Decarbonising road transport plays also a crucial role in the improvement of air quality in cities, which remains a fundamental challenge for public health. Indeed, air pollution is the reason of more than four hundred thousand premature deaths per year in Europe (EEA, 2016).

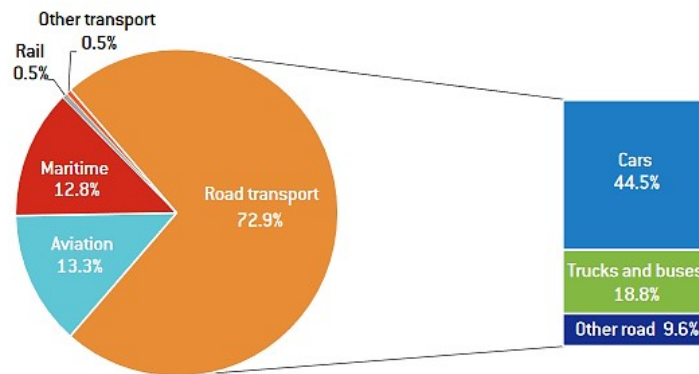


**Figure 1.2:** EU Transport greenhouse gas emissions by mode, 2015 (Source: Bruegel based on EEA)[1]

As previously discussed, with lower emissions requirements and improvements in technology, there has been an increase in the amount of research being conducted on fuel delivery systems, combustion systems, and exhaust after-treatment techniques, in order to meet new regulations.

A large number of different air pollutants are emitted by vehicles. These can be split into two groups: those that are regulated by EU transport legislation and those that presently are not. Pollutants that are not regulated by vehi-

cle emission standards in the EU include: certain acidifying pollutants, such as  $\text{NH}_3$  and  $\text{SO}_2$ ; certain carcinogenic and toxic organic pollutants, such as polycyclic aromatic hydrocarbons, persistent organic pollutants (POPs), dioxins and furans; and heavy metals, such as lead, arsenic, cadmium, copper, chromium, mercury, nickel, selenium and zinc [2].

The “regulated” pollutants include: hydrocarbons (HCs), carbon monoxide (CO), nitrogen oxides (NOx) and particulate matter (PM). *Table 1.1* summarizes the criteria and regulations imposed over the past 25 years for the emissions of gasoline engines in Europe.

		Positive ignition engines (Gasoline)							
		EU-1 1992	EU-2 1996	EU-3 2000	EU-4 2005	EU-5a 2009	EU-5b 2011	EU-6b 2014	EU-6c 2017
CO	mg/km	2720	2200	2300	1000	1000	1000	1000	1000
NOx	mg/km			150	80	60	60	60	60
THC	mg/km			200	100	100	100	100	100
NMHC	mg/km					68	68	68	68
PM	mg/km					5	4.5	4.5	4.5

*Table 1.1: Regulations of pollutants under EU legislation [3]*

Carbon monoxide (CO) is a product of incomplete combustion, which occurs when the carbon in the fuel is only partially oxidised, forming CO and not  $\text{CO}_2$ . It is a climate-altering agent: it does not pollute since it is something present in nature, also emitted by breathing and used by plants for photosynthesis. The problem therefore derives from its excess, which breaks a natural balance and leads to climatic alterations of which we are seeing the effects every day. It

also contributes to the formation of ground-level ozone and smog.

Nitrogen oxides ( $\text{NO}_x$ ), composed of nitric oxide NO and nitrogen dioxide ( $\text{NO}_2$ ), are all formed by the reaction of nitrogen with oxygen. It occurs mostly when temperature and pressure are elevated: in addition to burning fuel, oxygen starts to react also with the nitrogen of the air. They are instead included in the pollutants, since they are irritating to the respiratory tract. Furthermore, they contribute to the acidification and eutrophication of waters and soils.

Particulate matter (PM) generally includes both solid and liquid carbon particles emitted by the exhaust, result from agglomeration or crackling. They have many harmful effects both on the environment and on public health. Environmental effects include visibility impairment, aesthetic damages to stone and other materials. The impact on human health is of particular concern. These fine particles can be of various types and with different diameters:  $\text{PM}_{10}$  can penetrate to the larynx, while  $\text{PM}_{2.5}$  arrives in depth to the lungs and is therefore more harmful. The introduction of direct injection to the gasoline engine has meant their PM emissions are no longer insignificant (compared to earlier PFI engines) and has led regulatory bodies to begin imposing emissions limits on particulate mass.

Hydrocarbons (HCs) are substances which are produced by incomplete or partial combustion and are toxic to human health. They are regulated either as total hydrocarbon emissions (THC) or as non-methane hydrocarbons (NMHC). This term is used to describe the amount of the measured hydrocarbons impurities present.

As it can be seen in *Figure 1.3*, the levels of these allowable emissions greatly reduced over the years and further reductions are planned. However, real driving emissions can

be much higher than estimated by lab test results. Emission measurement made on the road showed that vehicles can have much higher emissions, especially with the critical PM and NO<sub>x</sub> emissions.

As a result of this, reducing type approval limits, like in the past, does not work effectively anymore. Therefore, the emission control process has been changed. Since September 2014, indeed, regulatory bodies have introduced Real Driving Emission (RDE) test: under RDE, a car is driven on public roads and exposed to a wide range of different conditions; specific equipment installed on the vehicle collects data to verify that legislative limits for pollutants such as NO<sub>x</sub> are not exceeded. This is the reason why, as it is outlined in the graph of *Figure 1.3*, since 2009, the trend of the approval limits in pollutants emission has suffered a freeze.

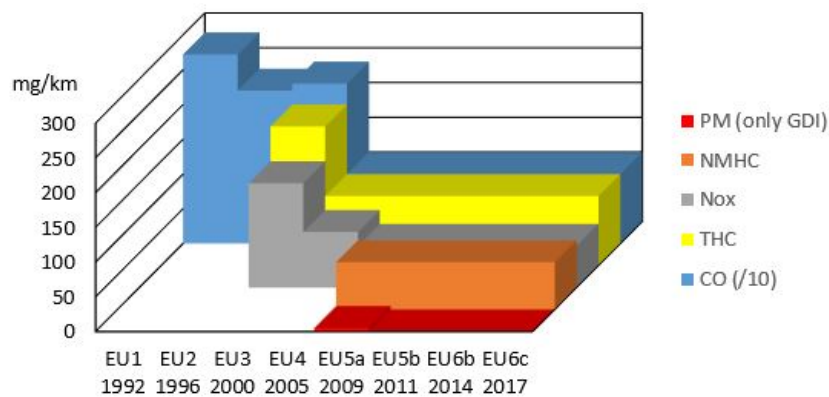


*Figure 1.3: Trend of pollutants regulations in EU (Data Source: EEA) [3]*

## 1.2 State of art in various propulsion methods

Internal combustion (ICE) engines are heat machines that convert most of the energy released by burning fuels into

mechanical work. The purpose of this kind of engines is the production of mechanical power from the chemical energy contained in the fuel-air mixture.

In internal combustion engines, as distinct from external combustion engines, the energy is released by burning or oxidizing the fuel inside the engine. Hence, the “internal” term indicates that the combustion takes place inside the machine, without resorting to external components in which the oxidation reaction could occur.

Due to their compactness, simplicity and high power-to-weight ratio, these engines have quickly established themselves as propulsion systems for transport vehicles and as power generators. They can be classified in various ways: depending on the way the combustion of the working fluid is started, the duration of their cycle, the nature of the fuel used, the air supply, the fuel supply, the cooling system. Nonetheless, reference is mainly made to the first classification criteria: according to this, internal combustion piston engines can be classified into spark-ignition (SI) engines and compression-ignition (CI) engines.

The spark-ignition engines, also known as Gasoline engines, use spark to ignite the fuel. In compression-ignition engines, instead, the air is compressed within the cylinder and the heat of this compressed air is used to ignite the fuel. They are also known as Diesel engines.

Although this work will thoroughly discuss gasoline engine development in depth, it is essential to firstly compare the context of gasoline to diesel engines, in terms of the current state of art and expected future developments.

### **1.2.1 Gasoline engines**

Gasoline internal combustion engines have dominated the global market in vehicle propulsion since the inception of

the motor vehicle. It is likely that the gasoline engine will continue to play a key role in vehicle propulsion for the foreseeable future.

In these engines, a mixture of air and fuel is ignited by a spark fired between the electrodes of a spark plug, thus achieving a very rapid combustion (ideally at constant volume). For historical reasons these engines are also called “Otto engines”, because of their inventor, the German Nikolaus Otto, in 1876.

### **1.2.2 Diesel engines**

Diesel powered vehicles have been around since the inception of the motor vehicle, like the gasoline ones. However, at the beginning, the diesel engine was not common to use in the passenger vehicle market, due to the higher price of cost production of its components. In recent times, instead, the number of passenger cars powered by diesel has grown such that they have overtaken gasoline engines as the most common propulsion method for cars in Europe.

Combustion in diesel engine differs fundamentally from combustion in the gasoline engine. In the gasoline engine, a mixture of air and fuel vapor is compressed and ignited by a spark shortly before top dead centre (TDC). In a diesel engine, instead, only air is compressed by the piston and the fuel is injected into the chamber towards the end of the compression stroke. At this point, the temperature and pressure of the air is high enough to cause the fuel to ignite spontaneously.

## **1.3 Classification and properties of fuels**

A fuel (from Old French *feuaile*, from Middle English *feuel*, ultimately from Latin *focalia*) is a chemical that may be ox-

idized in a combustion process, an oxidation reaction, producing thermal energy. Energy is a basic need to humans. Fuels, and energy in general, are used for heat generation, for work generation, or for chemical transformations. A common problem to all human needs is that energy is not available at the location and time we desire and sources must be found. Oxygen in the air is the basic oxidant for fuels: nitrogen is basically inert, although it combines endothermically with oxygen at high temperatures to get the unwanted NOx pollutants. The most abundant element on Earth's crust is oxygen, with 47%wt. It is also the most abundant in the hydrosphere, 86%wt. In the atmosphere it is second to nitrogen, with 23%wt. Oxygen is then readily available from Earth's atmosphere: that is why it is the main oxidiser for fuels. On the contrary, fuels are scarce and difficult to handle: the resources are unevenly spread all over the world and fossil sources are being depleted. In relation to the physical state in which they appear, fuels are classified as solid, liquid or gaseous. Another important distinction of fuels is between "natural" or "derivatives", in relation to the conditions in which they are used and according to their origin: natural (e.g. methane) if they are used as they are found in nature or derivatives (e.g. gasoline, LPG) if they are products of the transformation of natural fuels or of particular industrial processes. The fuels of major technical interest are organic compounds constituted by mixtures of hydrocarbons (i.e. organic chemical compounds of carbon and hydrogen atoms, and maybe some additional ones). It may be possible to find them also under the name of fossil fuels. The most important properties of fuels for the aims of this Thesis are the volatility and the octane number.

### 1.3.1 Volatility

Volatility represents the ability of a liquid to vaporize. In general, substances are considered volatile when, under certain conditions of pressure and temperature, they present high vapor pressure. In *Figure 1.4*, it is evident how the pressure vapor of a substance depends on temperature, pressure and kind of fuel.

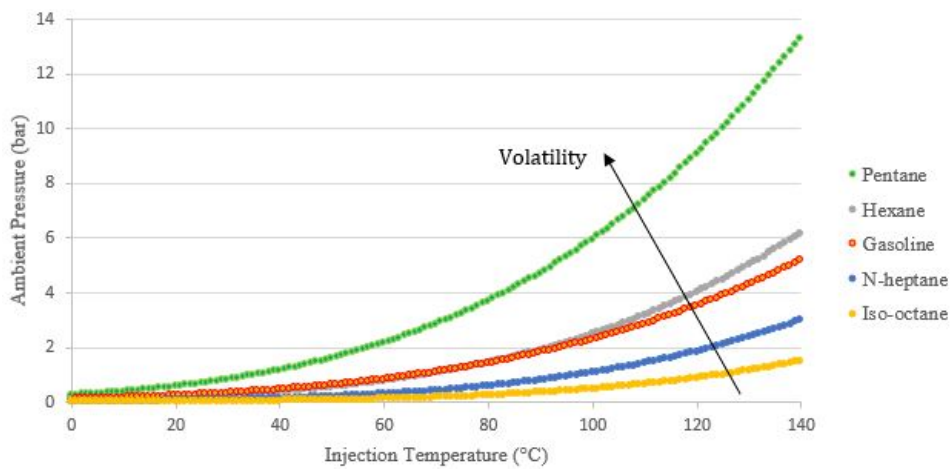


*Figure 1.4: Saturation pressure curves of different kinds of fuels*

More particularly, for fossil fuels, volatility affects engine starting, length of warmup period, fuel distribution, and engine performance.

Before going to discuss the ways in which volatility can affect engine operation, *Figure 1.4* and *Table 1.2* both show that volatility is inversely proportional to the number of carbon atoms present in the substance. The reason for this is that carbon atoms present molecular mass 12-fold greater compared to the one of hydrogen atoms: this means that the more carbon atoms there are, the less volatile will be the substance.

### Gas Fuels

<i>Methane</i>	CH <sub>4</sub>
<i>Ethane</i>	C <sub>2</sub> H <sub>6</sub>
<i>Propane</i>	C <sub>3</sub> H <sub>8</sub>
<i>Butane</i>	C <sub>4</sub> H <sub>10</sub>

### Liquid Fuels

<i>Gasolines</i>	C <sub>5</sub> - C <sub>9</sub>
<i>Pentane</i>	C <sub>5</sub> H <sub>12</sub>
<i>Hexane</i>	C <sub>6</sub> H <sub>14</sub>
<i>n-Heptane</i>	C <sub>7</sub> H <sub>16</sub>
<i>Iso-octane</i>	C <sub>8</sub> H <sub>18</sub>
<i>Kerosene</i>	C <sub>10</sub> - C <sub>13</sub>
<i>Diesel</i>	C <sub>12</sub> - C <sub>20</sub>
<i>Fuel Oils</i>	C <sub>14</sub> - C <sub>30</sub>

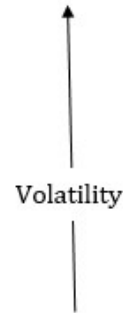


**Table 1.2:** Classification of fossil fuels

The volatility must be high enough to avoid excessive heat consumption due to evaporation, and yet not too high, to avoid losses or formation of vapor bubbles in the pipes.

If the fuel, too volatile, is completely in the vapor state, the rich mixture required during the acceleration phase would cause a reduction of power and an irregular functioning. Indeed, if the fuel is more volatile, it means that it evaporates more than another, under same thermodynamic conditions. In order to evaporate, it absorbs heat from the external environment (in this case, the combustion chamber, during the atomization phase). Hence, if the evaporation is enhanced, the amount of heat absorbed by the fuel in order to evaporate increases. In this case, the engine would cool down. In the acceleration phase, the need is maximum temperature and pressure in the combustion chamber for the maximum efficiency. For this reason, during this phase, the engine would

suffer a deterioration of the efficiency with enhanced evaporation.

Instead, in other regimes, high volatility of the fuel would lead to a reduction of size of the particles of the spray, thus leading to a better quality of the combustion process (decreasing pollutant emissions), and better atomization, improving the quality of the combustion and the overall efficiency.

As evidence of the key role played by the volatility in the modern research field, the fact that, if the fuel is not volatile enough, incomplete combustion is easily achieved and residues pass to pollute the lubricant.

### **1.3.2 Octane number**

The octane number indicates the tendency of a gasoline to self-ignite as the compression ratio in an internal combustion engine increases: it is a quantitative measure of a fuel mixture's resistance to "knocking."

The octane number of a certain fuel is measured on the basis of a standard blend of n-heptane, which has 0 octane, and iso-octane, which has 100 octane. The percent of iso-octane that leads to the same "knock" intensity as the sample is indicated as the octane number. For instance, a gasoline having an octane number 95 has the same resistance to detonation as a 95:5 mixture of iso-octane and n-heptane.

Two octane numbers are routinely used to simulate engine performance: Research Octane Number (RON) simulates gasoline performance under low severity (at 600 rpm and 49°C air temperature), while the Motor Octane Number (MON) is measured under more severe conditions (at 900 rpm and 149°C air temperature).

Road Octane Number (RdON) or Pump Octane Number (PON) or Anti-Knock Index (AKI) is the average of the val-

ues measured in the RON and MON tests. In *Table 1.3* the AKI values of the most significant fuels are set out.

<i>Fuels</i>	<i>AKI</i>
<i>N-heptane</i>	0
<i>Diesel fuel</i>	15-25
<i>Iso-octane</i>	100
<i>Ethanol</i>	116

*Table 1.3: AKI numbers of the principal fuels*

In spark-ignition engines the self-ignition of fuel must not take place before the spark plug ignition, to avoid the so-called *knocking* or *pinging* (*Figure 1.5*): hence, in this kind of engines, the octane number must be as high as possible.

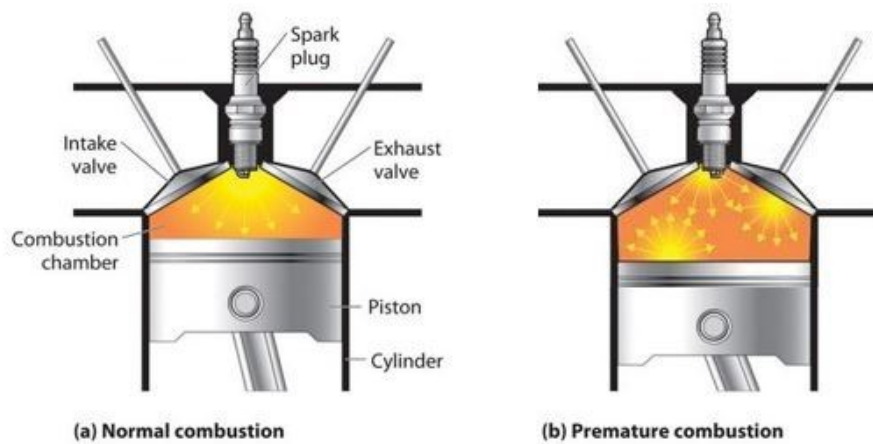


*Figure 1.5: Difference between normal combustion triggered by the spark plug (a) and detonation events (b)*

Usually, detonation occurs in the squish areas close to the exhaust valve, but it can occur in any area where conditions are favourable for its development. In practice, this phenomenon happens in the warmer areas of the chamber (heat is a trigger): thus, if the piston head or the exhaust valves

are not correctly cooled, they are the first candidates to be damaged.

In the normal combustion, for a perfect mechanical resonance and limited fuel consumption, the burst of the fresh charge takes place at a fixed position of the piston: the TDC (top dead centre). Throughout the knocking process, instead, the ignition of one or more fuel cores occurs in areas far from the spark plug, leading to the damage of the engine. Indeed, during the detonation events, there are very rapid increases in pressure in the combustion chamber which not only lead to a marked loss of power, but above all, cause damage to the pistons until they break (*Figure 1.6*).



**Figure 1.6:** *Piston heavily damaged by detonation; at this stage, the integrity of the engine is at risk*

The most damaging condition for the knocking to occur in an Otto cycle engine is a high load at a low speed. In fact, by accelerating abruptly to a very low engine speed, the most favourable conditions for detonation are reached. High pressures and low turbulence intensity of the gases are obtained in the combustion chamber.

Thus, to increase the octane number, anti-knock substances are added to the gasoline mixtures: by owing a greater octane

number, these substances lead to a knock retardation.

Prior to the 1970s, tetra-ethyl lead (TEL) was added to increase the octane number; this substance was subsequently removed because, unfortunately, turned out to be damaging for both catalytic converters and public health. Methanol, on the other hand, cannot be used because it has a corrosive action and dissolves gums and gaskets. Therefore, the only substance that can be used to increase the octane number having no catastrophic consequences is ethanol, which, however, due to its calorific value, tends to reduce engine performance in terms of km/liter.

## Chapter 2

# Gasoline Direct Injection Engines

This section will discuss gasoline direct injection engines, which are supposed to play a key role in the next 50 years, in the area of road vehicle propulsion.

### 2.1 Introduction

In the future passenger vehicles marketplace, gasoline fuelled engines will continue to play a main role and further research is essential to reduce their emissions and fuel consumption while maintaining driveability. As automakers around the world have been tasked with delivering more fuel-efficient vehicles, they have been able to put together more efficient engines. One technological advancement involves the deployment of a modified gasoline engine configuration that has been widely adopted: Gasoline Direct Injection (GDI).

The GDI engine started in aircraft applications, invented by the French inventor Leon Lavavasseur, in 1902. GDI engines were used extensively during the Second World War to power high output aircraft made in Germany, Soviet Union and US. The first automotive application of a GDI engine was developed by Bosch in 1952 [4].

Historically, the most widely produced gasoline internal combustion engines were of the Port Fuel Injected (PFI) design: in this kind of engine, the fuel is sprayed into the intake ports to mix with incoming air. The fuel injectors in PFI configurations are typically mounted in the intake manifold and the air/fuel mixture is pulled into the cylinder head as the intake valve opens.

In a GDI engine, instead, the fuel injectors are situated in the cylinder head and fuel is sprayed directly into the cylinder where the air / fuel mixing then occurs. The differences between the two configurations are easily visible in *Figure 2.1*.

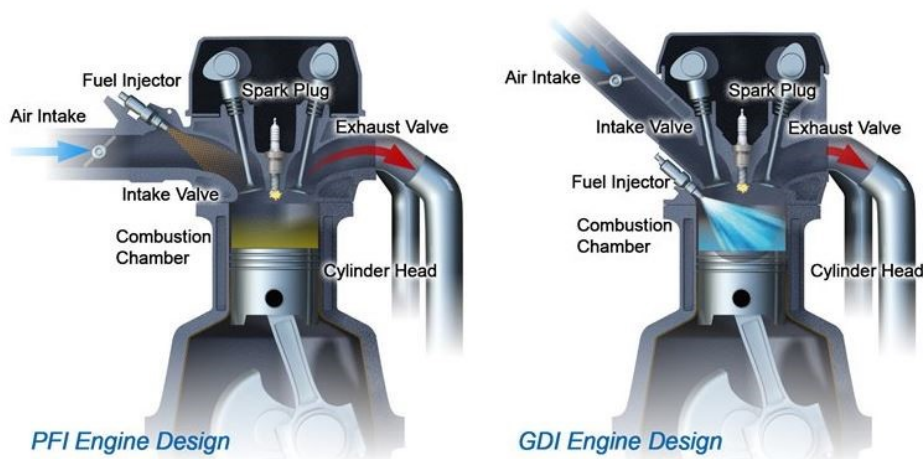


*Figure 2.1: Distinction between the configurations of gasoline fuelled engines: PFI (left) and GDI (right)*

There are many advantages of the GDI system over the PFI design, the most significant of which is better fuel economy. Due to these reasons, the global market has been changing over the past few years, as it can be seen in *Figure 2.2*.

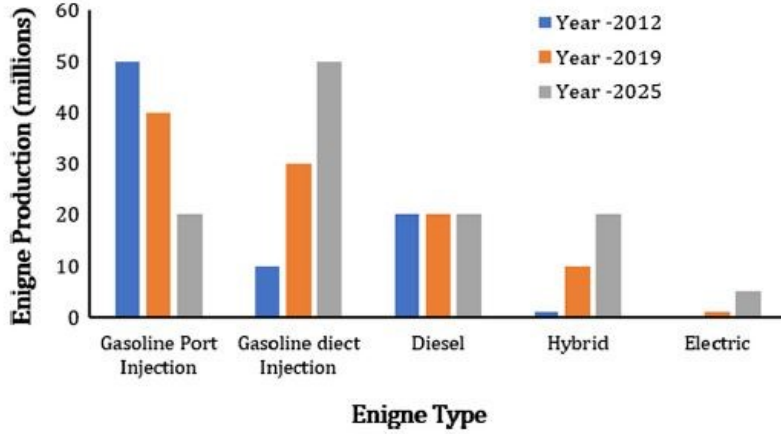


*Figure 2.2: Trend of the automotive propulsion global market throughout the years*

## 2.2 Operating principles

Under normal operating conditions a PFI engine would have fuel injected into the intake manifold during the intake cycle to mix with the air charge during the intake and compression strokes before ignition by the spark plug at a time close to the top dead centre (TDC). This means that the engine must always be run at close to stoichiometric conditions, otherwise the spark plug would not be able to ignite the air/fuel mixture within the cylinder.

This strategy is very suitable at high load conditions, where engine performance is the key parameter. However, at part and low load conditions, where fuel economy and low emissions are valued over the engine performance, this method is not ideal and running the engine in a lean burn mode would be preferable (*Figure 2.3*).

To control the airflow into the cylinder to ensure close to stoichiometric conditions, a throttle is used in PFI engines. However, large pumping losses are associated to this strategy. Gasoline direct injection engines (GDI) offer a potential so-

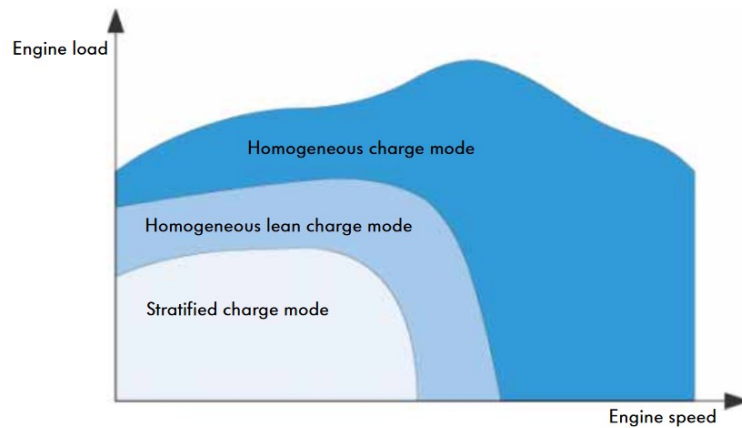


*Figure 2.3: GDI engine operating modes*

lution to this problem: GDI engine operates in two different modes, which are represented in *Figure 2.4*. The first GDI engine to operate in this two-stage mode was introduced by Mitsubishi, in 1998.

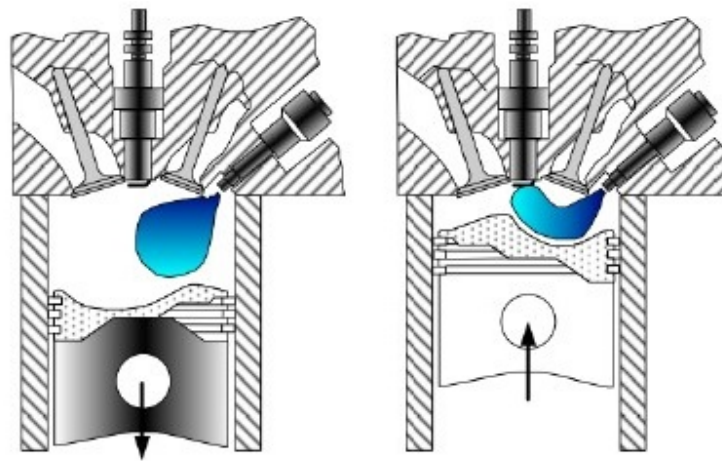


*Figure 2.4: Schematic representation of the homogeneous mode (left) and stratified mode (right) [5]*

At high loads the anticipated injection is carried out: the fuel is injected already during the suction phase to obtain a homogeneous and stoichiometric mixture (or rich if the power

must be maximized), in analogy to the PFI engines in every condition of load.

A GDI engine operating in homogeneous mode has a relatively long time for fuel/air mixing compared to the stratified charge operation mode. The fuel is injected during the intake stroke, so the mixing time comprises of the rest of the intake stroke plus the compression stroke.

Therefore, the right fuel/air mixing is governed by different factors, as follows.

1. By the ability of the fuel injector to deliver a finely atomised spray which is well dispersed around the cylinder without coming into contact with the cylinder liner and piston crown.
2. By the ability of the cylinder airflow to effectively distribute this fuel around the cylinder to form the most homogeneous mixture possible.

The overall combustion efficiency in homogeneous mode and the emissions levels are usually within allowed limits, but the overall efficiency in terms of power produced per unit mass of fuel is not as high as for stratified operation. Ideal injectors for homogeneous operation will spread the fuel as evenly as possible without impinging on the walls, so wide spray angle injectors are most desirable.

At part or low loads, a delayed injection is carried out: under stratified charge operation the fuel is only injected into the cylinder towards the end of the compression stroke, so the quality of the fuel/air mixing is much lower than that of homogeneous operation.

In this way, a stable combustion is realized which, for homogeneous mixtures with the same overall mixture ratio, could not be realized, due to the exceeding of the inflammation point. Although in the primary reaction zone there is a

local rich mixture, which would be associated with inefficient combustion and high emissions, the excess air in the cylinder provides a secondary reaction zone. To avoid the formation of fuel rich zones away from the initial reaction zone, which may not undergo efficient combustion due to flame quenching as a result of the burned gases, it is desirable to use an injector with a small spray angle.

### 2.3 Methods used for the stratification of the charge

For the stratification of the charge to be successful it is necessary to consider the air flow fields inside the cylinder, the time evolution of the spray and the combustion efficiency. There are different solutions for conveying the fuel near the spark plug electrodes. These are divided into three categories (*Figure 2.5*): *wall guided*, *air guided*, *spray guided*.

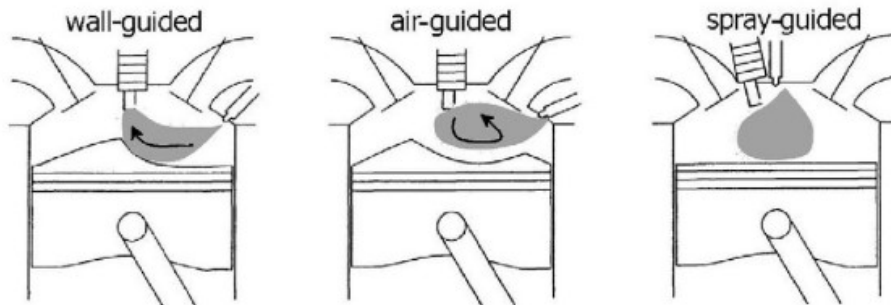


*Figure 2.5: Mixing stratification strategies*

In the wall guided solution, the fuel is guided through the geometry of the piston within the combustion chamber, towards the spark plug electrodes, also considering the appropriate positioning of the injector and the spark plug. With this solution the major problem is that of impingement since the impacted fuel with cold walls may not evaporate and

subsequently give rise to a high number of unburned hydrocarbons. Experimentally it has been seen that by injecting the fuel perpendicularly to the piston under conditions of temperature and ambient pressure, only 5% of the quantity injected forms a liquid film; in conditions of temperature and pressure typical of those of a gasoline engine, particles with a diameter of around 9  $\mu\text{m}$  are formed which, due to their small size, remain suspended and dragged by the air. Therefore, with this solution, it may be important to increase the distance between the tip of the injector and the spark plug electrodes so that even the impacted fuel on the wall reaches a right degree of evaporation before the mixture ignites.

The air guided solution is designed to solve the impingement problems of the previous solution as, in this case, the mixture will be stratified thanks to the air field, interposed between fuel and walls. This solution is difficult to implement since it is difficult to control the air motions in the combustion chamber, especially at low rpm when kinetic energy is reduced.

With the spray guided solution, it is attempted to carry out a self-confinement of the spray through the use of appropriate injectors to obtain a stable spray that is insensitive to air movements. However, this solution has a drawback: during the combustion phase the first combustion gases, expanding, bring the surrounding gasoline to come into contact with the walls, making it condense (*quenching*) and giving rise to the formation of unburned hydrocarbons.

This third solution is the main issue, but also primary objective of the realisation of this work. In *Table 2.1* is shown a comparison of the three different methods of fuel targeting that are shown in *Figure 2.5*. It should be stressed therefore that the distinction between the three solutions is purely theoretical, since, generally, in real systems the stratification of

the charge is obtained through an appropriate combination of these three methods.

	Advantages	Disadvantages
Wall guided	<ul style="list-style-type: none"> <li>• Highly stable as the fuel guide is a solid object, so relatively non-sensitive to spray characteristics</li> <li>• Distance from injector to spark plug along the path fuel takes is long, so atomisation quality is relatively good</li> </ul>	<ul style="list-style-type: none"> <li>• Increased impingement on piston crown, leading to fuel "pools" and therefore high HC emissions</li> <li>• Shaped piston is detrimental to desired airflow for homogeneous charge operation</li> <li>• Requirements for injector position are different from for homogeneous charge, hence a trade-off is made</li> </ul>
Air guided	<ul style="list-style-type: none"> <li>• Path of fuel from injector to spark plug is relatively long, ensuring a good level of spray atomisation</li> <li>• Reduced wall wetting, hence reduced HC emissions</li> </ul>	<ul style="list-style-type: none"> <li>• Sensitive to the engine flow field, which is highly changeable from cycle to cycle</li> <li>• Therefore requires matching between airflow and fuel spray which is a highly dynamic relationship</li> <li>• Engine airflow is not consistent over the full range of engine speeds</li> </ul>
Spray guided	<ul style="list-style-type: none"> <li>• Little variation in spray position at the time of ignition, so allows the highest level of stratification</li> <li>• Little dependence on engine airflow</li> <li>• Reduced wall wetting, hence reduced HC emissions</li> <li>• Ideal injector position is similar to that for homogeneous operation</li> </ul>	<ul style="list-style-type: none"> <li>• Injector and spark plug must be positioned close to one another</li> <li>• Distance from injector to spark plug is low, hence large drops and fuel bundles still exist at time of ignition causing high soot emissions</li> <li>• Sensitive to spray characteristics</li> <li>• Potential for mixture to be too rich local to the spark plug causing misfires</li> </ul>

*Table 2.1: Comparison of spray targeting methods*

## 2.4 Spray injectors in GDI engines

A spray is, in general, a dynamic collection of drops dispersed in a gas. The process of forming a spray is known as atomization and the spray nozzle is the device used to generate a spray. The two main uses of sprays are to distribute a liquid over a cross-section area and to generate and increase liquid surface area.

In this case, a fuel spray is a collection of fuel drops with

specified chemical and physical properties. The fuel spray from a GDI injector is essential to the proper functioning of the overall combustion process. The fuel injector has the key role of ensuring the fuel is metered precisely and is delivered into the cylinder at the correct position and at the right time, with the requested injection pressure, in order to ensure that the fuel will be correctly distributed at spark timing.

Several different types of fuel injector have suitable characteristics for a proper use in GDI engines. In the homogeneous mode, the ideal fuel injector will be able to produce a well distributed fuel spray with minimal amounts of wall wetting. Meanwhile, in the stratified charge mode it is more recommended to use a fuel injector which can introduce a high volume of fuel into the cylinder in a relatively short time towards the end of the compression stroke.

The three main types of injector which have been used in GDI engines are: the hollow-cone pressure swirl injector (which was the original injector used for GDI engines), the multi-hole solenoid injector and the piezo injector. They have been described more in depth in the next three sections and are represented in *Figure 2.6*.

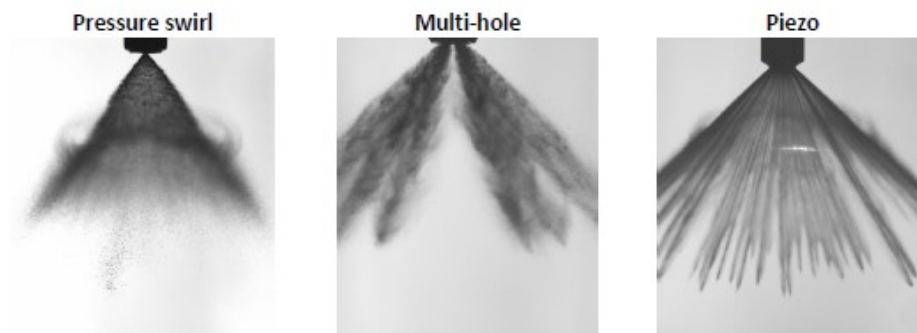


*Figure 2.6: Spray from different types of GDI injector*

### 2.4.1 Pressure swirl injectors

Swirling injectors have been commonly used for various combustion systems such as gas turbine engines, boilers and internal combustion engines to successfully mix fuel and oxidants with relatively low injection energy [6]. The pressure swirl injector has perfect characteristics of mixing and atomization mostly for engines with the requirement of continuous throttling [7].

For the GDI engines, this kind of injectors has been dominantly used because of its enhanced atomization characteristics through the break-up of a conical liquid film, which is initially formed inside the nozzle.

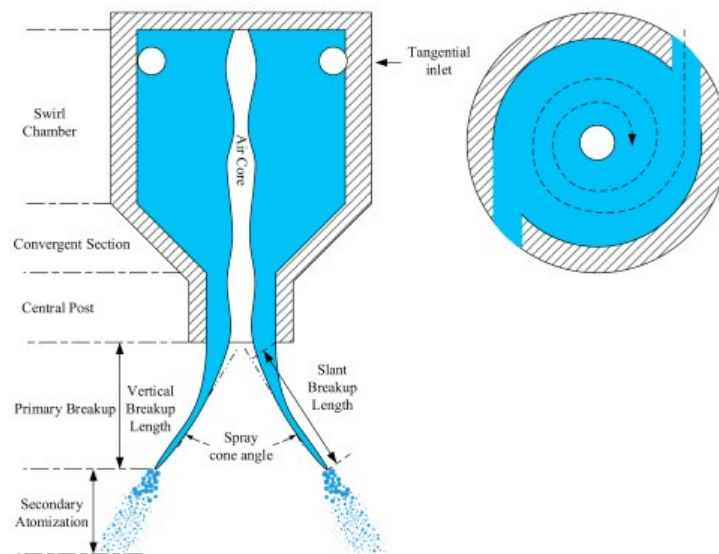


*Figure 2.7: Pressure swirl injector geometry of a liquid rocket engine*

In general, the operating principle can be seen in *Figure 2.7*. Fuel is introduced into the injector through several tangential orifices, such that within the injector body the fuel is swirling around the needle. When the needle is opened,

a continuous film is discharged from the perimeter of the outlet orifice producing a characteristic hollow cone spray pattern. Air or other surrounding gas is drawn inside the swirl chamber to form an air core within the swirling liquid. The generated spray maintains the swirling motion imparted by the tangential ports and an axial flow velocity due to the pressure of the fuel inside the injector. With this hollow-cone configuration, the average droplet diameter that can be achieved is of the order of 10-20  $\mu\text{m}$ : pressure swirl injectors are then high-performance devices which can guarantee very small drop size and, thus, a good mixing.

#### **2.4.2 Multi-hole solenoid injectors**

Pressure swirl injectors have been replaced in most applications by multi-hole injectors mainly due to the repeatability of their spray shape over a range of ambient pressure conditions. These are devices in which high pressure fuel is held inside the injector and when the needle is opened the fuel exits through a number of holes (normally between 5 and 10), usually of the diameter of 100-200  $\mu\text{m}$ . The fuel pressure is the key driver to force the passage of the fuel through the holes. The needle is operated by a solenoid, which is supplied by current. The metal needle is opened when it is magnetically attracted by the solenoid, supplied by current: in this way, the injector will be opened and the fuel forced through the holes. Rather, the needle is shut when the solenoid current is released and a spring forces the needle back to the closed position. The average droplet diameter for multi-hole injectors is 5-6  $\mu\text{m}$ . The internal arrangement can be seen in *Figure 2.8* and the resulting spray is shown in *Figure 2.6*.

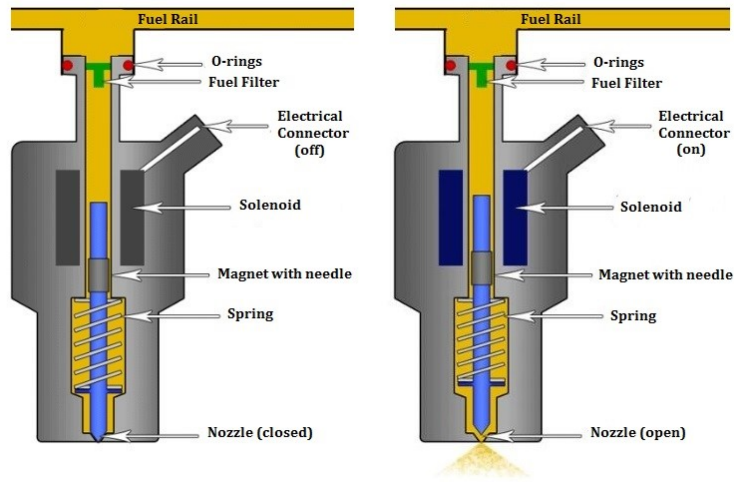


*Figure 2.8: Multi-hole solenoid injector geometry*

### 2.4.3 Multi-hole piezo injectors

The piezo electricity is the characteristic by which some crystals, quartz or topaz, like crystal ceramic, can be electrically loaded through a mechanical deformation, or alternatively can change shape when submitted to an electrical field action. Piezo injectors work on many of the same principles as solenoid driven injectors, however, the injector is operated by a piezoelectric stack, as represented in *Figure 2.9*. These injectors work by passing electrical current through a stack of piezo crystals, causing it to expand; as the crystal discharges the current it contracts to the original size (piezoelectric effect). To obtain a useable degree of displacement, it requires a stack of no fewer than 400 ceramic disks to form the active element of the injector. The expansion and contraction of the crystals displaces the fuel within the injector, causing the needle valve to open and close extremely quickly and precisely. The fuel spray shape at the exit of the nozzle is shown in *Figure 2.6*.

The major advantage of piezoelectric injectors is their speed of operation (up to five times faster than conventional

electrohydraulic solenoid injectors) and the repeatability of the movement of the valve. The dilation and retraction movements of the piezoelectric elements are almost instantaneous. This reaction speed allows even more precise proportioning of the injected fuel and a greater number of injections per cycle. Therefore, using this kind of injector higher injection pressures may be reached. Due to the cost of the piezoelectric cells these injectors are orders of magnitude more expensive than their solenoid driven counterparts so are only used in the luxury car market. The average diameters of droplets with piezo injectors are 3-4  $\mu\text{m}$ .

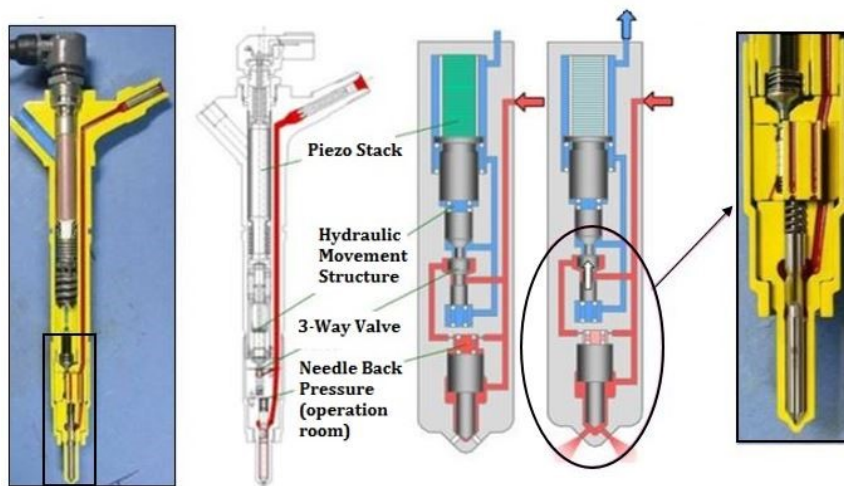


*Figure 2.9: Internal geometry of a piezo injector*

## 2.5 In-cylinder charge air motion

The process in which the fuel is mixed with the air inside the combustion chamber is essential for the effective operation of the engine and it represents the in-cylinder charge air motion. In internal combustion engines, especially in Diesel engines and GDI, the in-cylinder turbulent flow plays a fun-

damental role, defining engine performance and efficiency [8]. This is caused by the fact that this kind of engines requires an optimal mixing within the chamber, since it is not possible to anticipate the mixing between fuel and air before the injection in the chamber, as it happens in the PFI engines.

During the flow introduction, a large-scale turbulent structure is created and includes high levels of turbulence. Kinetic energy is stored in the large-scale motion and, during the compression, is regarded to dissipate into smaller-scale turbulent flows, which enables faster burning rates for optimal combustion. During homogeneous operation it is aimed to have the fuel evenly distributed throughout the cylinder prior to combustion. High levels of turbulence are vital to this process. For stratified operation, turbulence is also essential to ensure a short combustion event and for the dilution of undesired combustion products.

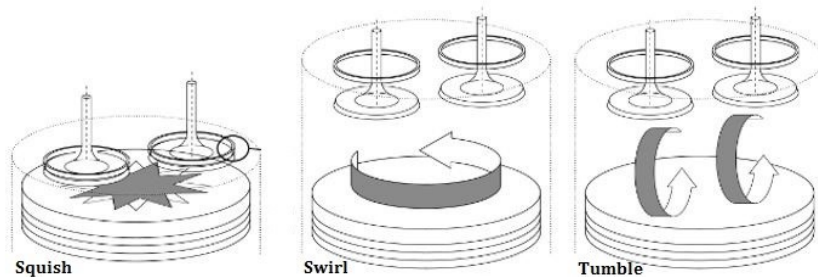


**Figure 2.10:** *Phases of the turbulent flow in the combustion chamber*

The shape of piston crown and cylinder head and the operation of the valves are designed to induce organized and essential motions in the combustion chamber, known as *squish*, *swirl* and *tumble*.

As it has been simply modelled in *Figure 2.10*, the main difference between them is that swirl and tumble occur dur-

ing the suction phase, while the squish takes place when the piston meets the cylinder head. In the next sections they are developed and explained deeper [9].

### 2.5.1 Squish

This term refers to the rotational movement performed by the charge on an axial plane, which is generated towards the end of the compression phase, as a consequence of the unequal volume change available for the fluid, when the piston crown approaches significantly the cylinder head in some areas and for some particular shapes of the piston crown.

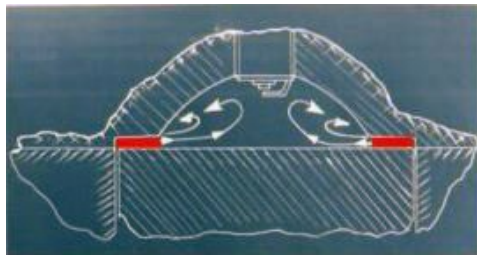


*Figure 2.11: Squish generated by the shape of the cylinder head*

In particular, in spark-ignition engines, it is the conformation of the cylinder head that generates the squish (*Figure 2.11*), while in compression-ignition engines it is the cup formed in the piston that produces a double vortex of squish at the end of the compression phase. In short, it is the movement of the mixture which, squeezed between the piston and the head, moves rapidly from the peripheral zone towards the centre and the spark plug. It is very important and sought since it is able to reduce the danger of detonation and self-ignition, promotes mixing around the spark plug and ensures subsequent better combustion.

### 2.5.2 Tumble

This term indicates a rotary motion organized on a plane passing through the axis of the cylinder, which begins to form during the suction phase and is then supported and amplified towards the end of the compression phase (*Figure 2.12*).

Also using a normal traditional type duct, a vortex is formed on an axial plane in the area below the valve plate during the suction process. It is the consequence of the interaction of the incoming flow with the cylinder wall (from the exhaust side) and the piston head. In fact, during the suction phase, a rotary motion is formed, organized in a single vortex on an axial plane. During the subsequent compression phase, the rising of the piston "crushes" the vortex, reducing its size and increasing its intensity (kinetic energy).



*Figure 2.12: Tumble*

To accelerate the tumble, it is therefore necessary to design a duct that not only accelerates the incoming flow, but also directs it mainly towards the area below the discharge valve. The main advantage of the tumble consists therefore in the ability to generate turbulence towards the end of the

compression stroke so as to accelerate and stabilize the initial part of the combustion process. On the other hand, it must be kept in mind that the energy expended to increase the tumble during the suction phase ends up penalizing increasingly the filling of the cylinder. Tumble is especially important in spark-ignition engines. However, this motion is unstable, extremely difficult to control.

### 2.5.3 Swirl

Swirl is characterized by motion around the cylinder axis (*Figure 2.13*). It is mainly influenced by the geometry of the intake-duct group. This is easier to manage and more stable than the tumble motion. Normally this turbulence can be created in two different ways:

- through the interference of the incoming flow with the cylinder wall or with a screen placed on the valve itself;
- by giving the incoming flow a rotary motion around the same axis of the valve before entering the cylinder.

In the second specific case, oriented or helical ducts are used. With the geometry-oriented ducts it is the story to be given to the jet coming out of the valve of a non-uniform speed distribution on the circumference, so as to orient the flow towards the cylinder wall, which in turn imposes itself in a Swirl bypass. With the helical ducts the fluid arrives with a strong tangential component in the area above the light discovered by the valve and from here then descends with rapid helical movement towards the cylinder. The oriented ducts, however, tend to be not very effective as swirl generators at the small risers from the moment in which the fluid speed in the suction operation is too low thanks to its particular geometry could impose an unequal flow distribution along

the periphery of the valve. All the higher rises are, on the other hand, very effective in order to produce swirl but have low flow coefficients since it is used to dispose of a portion of the light area discovered by the valve. An improvement from this point of view is obtained with the helical ducts through which it is necessary to have flow coefficients significantly better than those offered by a selection valve and swirl coefficients. Unlike tumble, it does not break down as the piston approaches TDC.

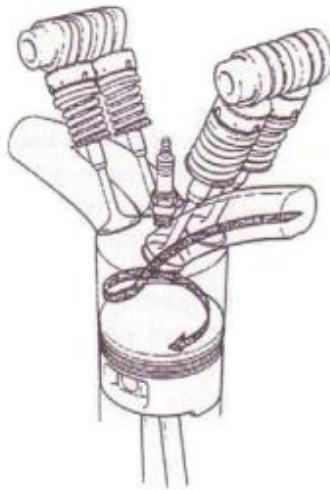


*Figure 2.13: Swirl*

The influence of both the motions has been investigated in a GDI engine and the tumble was found to be the strongest of the three bulk motions [10]. For this reason, it is suggested that where air-guiding is used for stratified operation a tumble dominated flow regime is used.

## Chapter 3

# Spray Atomization

As previously mentioned, the spray produced by the multi-hole injector is a key parameter of the efficiency of the engine and has an essential role in the emissions formation. For this reason, the spray, and therefore the injector, must be correctly sized in order to be coupled to the combustion chamber in the right way. In this chapter, it is explained how a GDI injector spray is characterised and the factors which contribute to the formation of a well atomized spray.

### 3.1 Spray structure

Sprays are complex fluid mechanical structures generated by the disintegration of a liquid sheet or jet into droplets in a surrounding gas. The global position of the spray in the combustion chamber is of vital importance as it must be dispersed suitably throughout the cylinder, thus forming a homogeneous mixture or, in the case of stratified mode, a region of combustible mixture in the vicinity of the spark plug at the time of the ignition. Nonetheless, it is essential that impingement on the cylinder walls and piston crown is minimal, as it leads to formation of pools and aggregates of fuel which will not fully combust and will form unburned hydrocarbon.

A spray produced by the multi-hole injector can be characterized according to a number of basic parameters such as temporal and spatial morphology, quality of mixing and the potential for that mixture to ignite in the desired manner within the combustion chamber. The spray basic parameters are described by referring to the *Figure 3.1*.

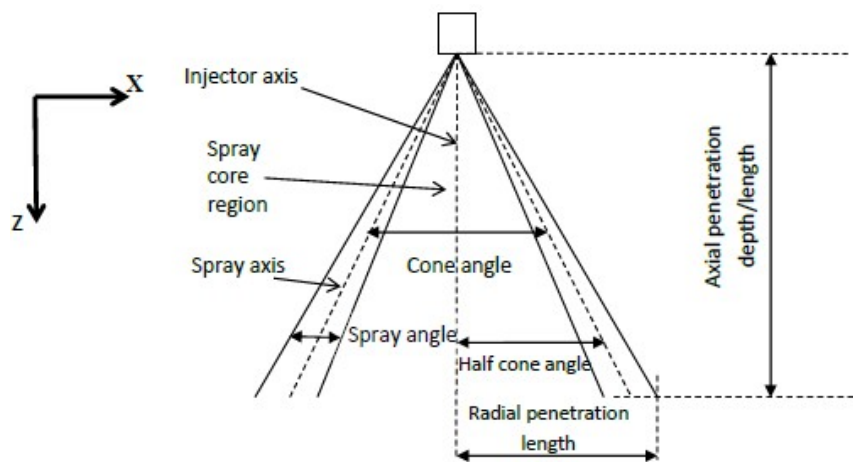


*Figure 3.1: Spray parameters*

Firstly, the penetration describes the distance from the nozzle exit to the instantaneous tip of the spray. The penetration may be measured axially or radially. The axial penetration is the one along the injector axis and it is the most commonly measured. The radial penetration is also essential to describing an injector and is measured perpendicular to the direction of the injector.

In the spray generated by a multi-hole injector, each hole produces a spray plume. The spray axis is the centre of each particular spray plume. For regular pattern nozzles, this should be the same as the axis of the nozzle hole, but due to cavitation changing the apparent nozzle angle and the pressure drop in the centre of the plumes this is not actually

the case [11].

The spray angle, or plume cone angle, is the angle between the extremities of a spray plume from the nozzle exit. For a multi-hole injector, each individual spray plume has an associated individual spray angle. This angle is extremely sensitive to the measurement location, as it is not constant in the plume direction.

The cone angle is the angle between the spray axis for two opposite spray plumes. Many multi-hole injectors do not have an even number of symmetrical holes, so definition of the cone angle is not as simple.

The spray footprint is the shape of the spray on a plane perpendicular to the injector axis.

### **3.2 Properties influencing spray formation**

The morphology of the spray is affected by the characteristics of injected liquid and ambient gas and by the geometry of the nozzle. The most relevant liquid properties to spray generation are viscosity, surface tension and density.

The viscosity represents the fluid resistance to flow, in other terms, the momentum exchange coefficient. It is the most important liquid parameter which control the atomization process, due to its effect on droplet size, liquid flow rate and the geometrical shape of the spray. Liquid viscosity is strongly dependant on the temperature and generally decreases with increasing in temperature [12]. The liquid surface tension is the second most important parameter in atomization, due to its property to resist liquid expansion. Liquids with high surface tension are more difficult to disintegrate by aerodynamic, centrifugal or pressure forces comparing to those of lower surface tension. In general, for most pure liquids in contact with air, the surface tension decreases

as temperature increases. Finally, the effect of the liquid density on atomization has been poorly investigated but, in general, it can be argued that more resistance to disintegration is expected for high density liquids.

In order to assemble all the aforementioned effects on spray formation and morphology, various dimensionless numbers may be useful: in fact, the physical modelling of spray is based on the use of Reynolds number, Weber number and Ohnesorge number.

The Reynolds number ( $Re$ ) gives a good indication regarding the state of a flow.  $Re$  is proportional to the inertial forces divided by viscous forces, as indicated:

$$Re = \frac{\rho v l}{\mu} \sim \frac{\textit{inertial forces}}{\textit{viscous forces}} \quad (3.1)$$

where  $\mu$  is the dynamic viscosity in  $\text{kg}/(\text{s}\cdot\text{m})$ ,  $\rho$  is the fluid density in  $\text{kg}/\text{m}^3$ ,  $l$  is the characteristic length scale in  $\text{m}$  and  $v$  is the velocity in  $\text{m}/\text{s}$ .

The non-dimensional Weber number ( $We$ ) is defined as the ratio of the inertial forces tending to break apart the liquid core to the surface tension forces tending to hold it intact. Its general form is given as:

$$We = \frac{\rho v^2 l}{\sigma} \sim \frac{\textit{inertial forces}}{\textit{surf tension}} \quad (3.2)$$

where  $\sigma$  is the surface tension of the liquid considered, in  $\text{N}/\text{m}$ . The Weber number is useful to classify the disintegration regimes of the spray.

The final dimensionless number of importance is the ratio of viscous friction and surface tension called the Ohnesorge number ( $Oh$ ), which is a combination of the  $We$  and the  $Re$ , as it can be seen in the equation:

$$Oh = \frac{\mu}{\sqrt{\rho\sigma l}} = \frac{\sqrt{We}}{Re} \sim \frac{\text{viscous forces}}{\sqrt{\text{inertia} \cdot \text{surf tension}}} \quad (3.3)$$

### 3.3 Disintegration process and spray break-up

Atomization refers to separating something into fine particles. It is a process of breaking bulk liquids into small droplets. The generation of droplets is a complex phenomenon governed by the opposition of surface tension of the liquid with external aerodynamic forces. Droplets are formed by the break-up of liquid ligaments (primary break-up) or by the disintegration of a large droplet into a multiplicity of small ones (secondary break-up).

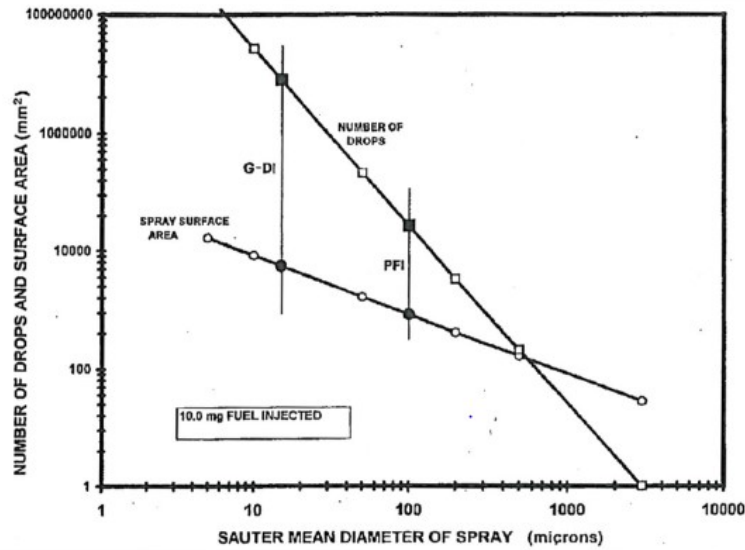


Figure 3.2: Correlation between break-up and surface area [14]

It is essential to atomise the spray to create a region with a large number of droplets, as this increases the overall sur-

face area of the spray, and thus the evaporation rate and combustibility of the spray. Therefore, it has been seen that a smaller mean drop size will usually correlate to a reduction in the levels of emissions product [13].

The correlation between reduced mean droplet diameter, increased number of droplets and overall surface area is shown in *Figure 3.2*. As represented in the figure, the typical spray morphology in a GDI engine is different from that one of a PFI: in a GDI injector, the size of spray is smaller, with a greater number of drops, thus increasing the overall surface area.

According to the combined effects of surface tension and aerodynamic forces, the break-up process of a jet may be classified into four regimes [15]:

1. Rayleigh break-up regime
2. First wind induced break-up regime
3. Second wind induced break-up regime
4. Fully developed atomization regime

Rayleigh break-up is initiated by viscous forces as opposed to aerodynamic forces and effectively causes the jet to form a dripping motion. This occurs for gas Weber number of below 0.4. Droplet diameters are much larger than the jet and are roughly two times the jet diameter [16].

First wind-induced break-up is the point at which aerodynamic drag has a greater effect on break-up than the viscous forces. The drag force also accentuates the oscillations generated by the viscous forces. This occurs for gas Weber numbers between 0.4 and 13. The droplets formed have a diameter of the order of the jet diameter. Second wind-induced break-up occurs when the aerodynamic forces further exceed the surface tension forces due to increased relative motion

between the air and jet. The break-up of the jet now occurs much closer to the nozzle and the drops are of significantly smaller diameter than the jet diameter. The gas Weber number for these conditions is between 13 and 40.3. The final stage of break-up is the atomization regime, which is characterized by the complete disintegration of the jet. The onset of break-up is on, or very close to, the nozzle exit and leads to the formation of a fine spray of very small droplets. This occurs for gas Weber numbers of over 40.3.

*Figure 3.3* shows the categorization of these regimes in terms of Ohnesorge number versus Reynolds number on a log arithmetic scale.

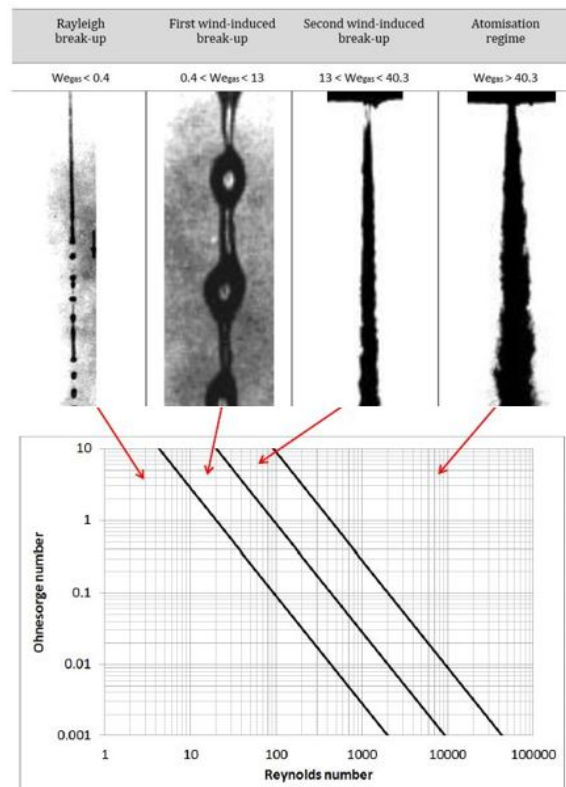


*Figure 3.3: Correlation between jet break-up regimes and Ohnesorge-Reynolds break-up diagram [17]*

## Chapter 4

# Developments in GDI Spray Research

Many studies about spray characteristics and breakup regimes in gasoline direct injection engines have been investigated. Nevertheless, spray behaviour under certain engine operation conditions is not completely understood. This section will focus on particular thermodynamic conditions, which represent both the potential basis of improvements in injection research field and one of the most serious problem to be solved in GDI engines.

### 4.1 Split injection strategies

In order to satisfy the increasingly strict emissions regulations, the injection and combustion systems must become ever more efficient. Various studies are being conducted to seek the optimal approach to improve the fuel efficiency. The use of split or multiple injection strategy represents the potential method to deliver these improvements.

Split injection means that the total amount of fuel injected in the chamber is separated in two or more short injections, with a separation time between the individual injection events, known as dwell time. This leads to advantages

like reduction in pollutant emissions, improved performance, noise reduction.

In order to augment the number of injections, new piezo-electric injectors have been used. Thanks to them, the time between one injection and the other has been reduced, from around  $1500 \mu\text{s}$  to  $150 \mu\text{s}$ . The other substantial variation lies in the minimum flow: being split in more injections, the minimum flow manageable turned from  $2 \text{ mm}^3$  to less than  $1 \text{ mm}^3$ .

Split injection strategies have been firstly used in diesel engines to control the heat release rate [18]. For instance, the Common Rail “Unijet” system for Diesel engines is able to manage two injection events for each cycle, depending on the chamber temperatures and on driver’s demand. The pilot injection is used to thermo-physically prepare the combustion chamber to the next principal injection. Indeed, as shown in *Figure 4.1*, the combustion of a small amount of Diesel is injected with a certain advance and contributes to increase the intern temperature and consequently the evaporation and the resultant atomization of the principal injection.

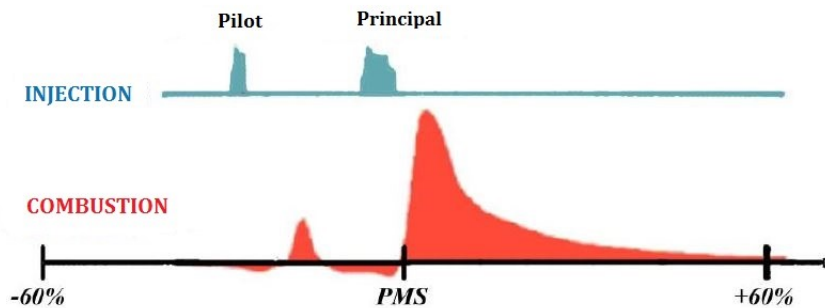


*Figure 4.1: Pilot and principal injection events in relation with the combustion phenomenon*

Furthermore, in the last year, as highlighted in the Introduction, the regulations on hydrocarbon (HCs) emissions are

being restricted and the main sources of this kind of emissions are pool fires caused by piston and wall wetting [19]. Indeed, the overlong penetration of the spray plumes could lead to the formation of the abovementioned pool fires, increasing the formation of HCs.

By splitting the fuel mass into a number of separate shorter injection events, the level of resistance between fuel and air is increased. This involves not only a shorter penetration of the spray plume but also an improved homogenization within the combustion chamber, particularly in the zone around the spark plug.

In summary, the effects of the split injection strategy become increasingly important due to the improved atomization and quicker enhanced evaporation [20].

## 4.2 Flash boiling process

During certain stages of GDI engines operation, the combination of increased fuel temperature and sub-atmospheric cylinder pressure during the injection can lead to a phenomenon called flash boiling. Put simply, the latter is the rapid formation and growth of bubbles inside droplets, which leads to the shattering of the droplets into many smaller droplets.

This process greatly affects the atomization process: hence, it is essential to develop an understanding of the effects on the morphology of the spray. Flash boiling has the advantage of achieving proper atomization at a lower cost compared with increasing fuel injection pressure. However, heavy flash boiling should be avoided, because of the consequences it leads: as it will be evident in the following, it involves spray collapse phenomenon with, consequently, major PM in the exhaust and more consumption, due to respectively major penetration length and reduced volume of the spray.

In the following section the conditions under which this process occurs are investigated, after an introductory paragraph focused on the differences between evaporation and flash boiling; thereafter, a description of the flash boiling mechanism is provided.

#### 4.2.1 Difference between evaporation and flash boiling

The phase transition between a liquid and a gas can occur through two opposite processes: vaporization and condensation. There are two types of vaporization: evaporation and flash boiling.

Evaporation is a phase transition from the liquid phase to vapor that occurs at temperatures below the boiling temperature at a given pressure. It occurs on the liquid surface.

Boiling is also a phase transition from the liquid phase to the gas phase, but boiling is the formation of vapor as bubbles of vapor below the surface of the liquid. Furthermore, in contrast to evaporation, the boiling is not a natural process. Boiling occurs when the temperature of the liquid is greater than the boiling point of the substance. Evaporation can occur at any temperature.

The most significative differences are listed in *Table 4.1*.

	<b>Flash Boiling</b>	<b>Evaporation</b>
<b>Definition</b>	<i>Vaporization of liquid into gas due to continuous heating. It is not a natural process.</i>	<i>Natural process in which the liquid changes into gaseous form, when there is an increase in temperature or decrease in pressure or both.</i>
<b>Occurrence</b>	<i>Large mass</i>	<i>Only on surface</i>
<b>Temperature to occur</b>	<i>It happens when the temperature reaches the boiling point</i>	<i>The temperature does not need to reach to boiling point</i>
<b>Bubble formation</b>	<i>Visible</i>	<i>Bubbles do not form</i>
<b>Length of the process</b>	<i>Rapid process</i>	<i>Slow process</i>

*Table 4.1: Main differences between evaporation and flash boiling*

Internal combustion engines rely upon the vaporization of the fuel in the cylinders to form a fuel/air mixture in order to burn well. Both the processes of vaporization and flash boiling can happen, although flash boiling conditions are more difficult to be encountered. Fuel droplets vaporize as they receive heat by mixing with the hot gases in the combustion chamber. Heat (energy) can also be received by radiation from any hot refractory wall of the combustion chamber. In *Figure 4.2*, the saturation curve of n-hexane is represented. As previously mentioned, flash boiling phenomenon can only happen when the temperature reaches the boiling point (saturation line), while evaporation can happen for each point at the left of the saturation line.

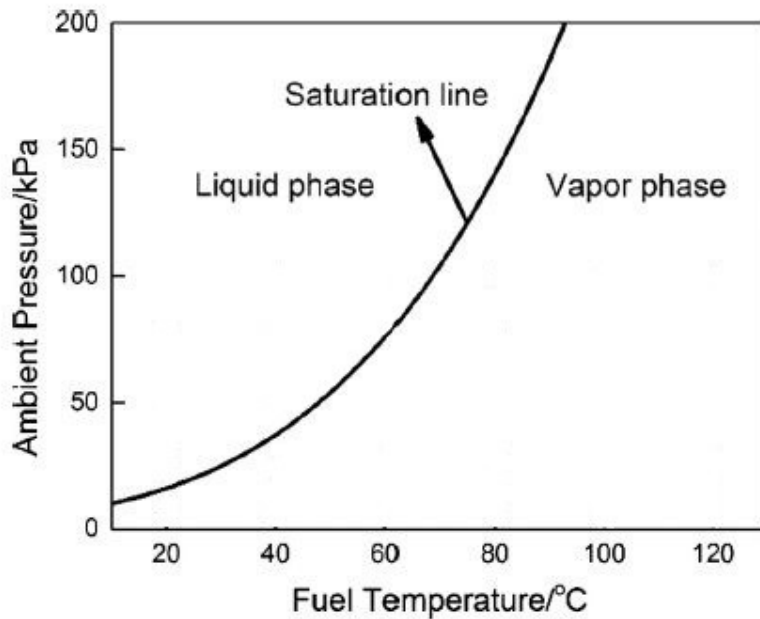


*Figure 4.2: Saturation line of n-hexane, from [21]*

#### 4.2.2 Conditions for the flash boiling to occur

As mentioned before, flash boiling is a phenomenon that occurs when the liquid fuel is injected in a chamber where the ambient pressure is lower than the saturation pressure of the fuel. This particular condition may occur especially during the acceleration phase. If the engine is operating under wide throttle openings (such as accelerating from a stop) then engine speed is limited by the load: engine speed is low but the butterfly valve is fully open, creating a very low pressure within the combustion chamber, with high temperature of the fuel. Therefore, flash boiling occurs when fuel is injected into the cylinder in a “superheated” state. The difference between the actual conditions and the minimum conditions required for flashing is known as superheat degree and can be defined either in terms of temperature or pressure, as shown in 4.1 and 4.2.

$$\Delta T = T_{fuel} - T_{sat} \quad (4.1)$$

$$\Delta P = \frac{P_{sat} - P_{amb}}{P_{amb}} \quad (4.2)$$

Herein,  $T_{fuel}$  is the fuel temperature,  $T_{sat}$  is the saturation temperature,  $p_{amb}$  corresponds to the chamber pressure and  $p_{sat}$  is vapor pressure (saturation pressure) of the fuel.

Hence, understanding when flash boiling process occurs and determining the strength of the effect means to identify the saturation pressure of the used fuel (at the corresponding fuel temperature) and comparing it with the value of the ambient pressure in which the fuel is injected.

### 4.2.3 Flash boiling mechanism: bubble nucleation and growth

The formation and growth of bubbles inside liquid fuel droplets is fundamental for the mechanism of flash boiling. It was found that there are three stages of flash boiling:

1. Bubble Nucleation
2. Bubble Growth
3. Two-phase flow

Nucleation is the first step in the formation of a new thermodynamic phase or a new structure, starting from a state of metastability. The kinetics of formation of the new phase, as the bubbles are, is frequently dominated by nucleation, such that the time to nucleate determines how long it will take for the new phase to appear. Bubble nucleation can be classified into two groups:

- Homogeneous
- Heterogeneous

The heterogeneous bubble nucleation depends on container walls and fluid impurities, so that it is impossible to characterise. However, heterogeneous nucleation is inevitable under superheated conditions in all the fuel injectors, given the interaction with the nozzle walls and the presence of fuel impurities. In conclusion, the heterogeneous nucleation is relevant inside the nozzle [22].

Nevertheless, in this work particular attention must be given to homogeneous nucleation, which is the process causing the creation of the bubbles within the spray in the combustion chamber. The classical nucleation theory (CNT) is the most common theoretical model used to quantitatively study the kinetics of nucleation. According to the latter, the

rate of formation of bubbles can be characterized by  $J$ , as in 4.3:

$$J = J_0 \cdot e^{\frac{-\Delta G}{k_B \cdot T}} \quad (4.3)$$

In which  $J_0$  represents an initial constant of the fluid,  $k_B$  the Boltzmann constant,  $G$  the Gibbs free energy cost of the nucleus and  $T$  the temperature (considered constant in the model).

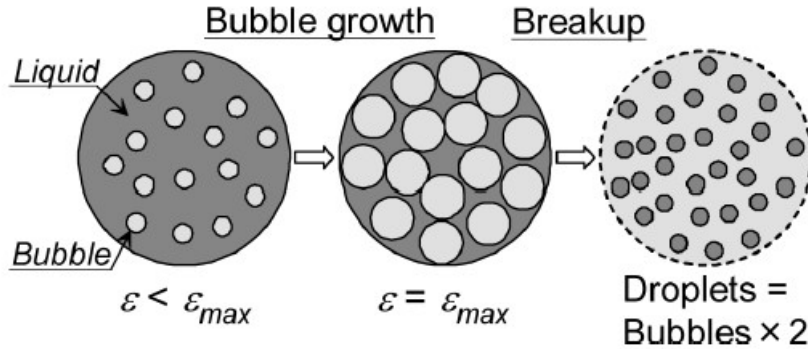


*Figure 4.3: Stages of bubble growth [23]*

The bubble growth process is analysed and summarised in *Figure 4.3* and it is based on the following assumptions:

- The temperature and pressure inside the bubbles are uniform and temperature is the same of the one of the liquid fuel.
- Bubbles grow spherically.
- Phase change from liquid to vapor occurs continuously.
- The coalescence due to the Marangoni effect is not considered in this model.

The bubbles grow through phase change from liquid to vapor. Hence, the ratio of bubble to liquid fuel increases.

It is now introduced the void fraction  $\epsilon$ , which describes the ratio of bubble to liquid within the droplet, as in 4.4.

$$\epsilon = \frac{V_{bubble}}{V_{bubble} + V_{liquid}} \quad (4.4)$$

Once bubble growth has caused the void fraction to reach a critical value, such that bubbles are interacting with one another, the droplet will shatter and form a cloud of many small droplets. The model of Kawano et al.[24] specifies that the number of droplets after shattering will be twice the number of bubbles prior to it. After this process has been completed a mixture of liquid droplets surrounded by vapor will exist. The momentum of the original parent drop will be distributed among the secondary droplets and so on, until a distribution of vapor and tiny droplets is created. It is so reached the disintegration of the liquid jet and therefore promoting fuel atomization.

#### 4.2.4 Flash Boiling in multi-hole injector sprays

Once microscopically analysed the way with which the flash boiling occurs, the focus is now on the effects of flash boiling on the macroscopic morphology of the spray.

Flash boiling, as aforementioned, has the advantage of achieving proper atomization at a lower cost compared with increasing fuel injection pressure. But heavy flash boiling, which should be avoided, would cause spray collapse. Flash boiling and its accompanying spray collapse phenomenon have become an exciting topic among researchers recently.

### 4.3 Spray collapse

Due to the variation of chamber physical conditions during engine operation, the plumes of which a spray is composed may undergo changes in their macroscopic shapes. These changes can affect the angles, the width or the penetration of the spray and the aim of the present work is not just detecting the variation of these parameters but also relating it to the physical effects of the spray.

Spray collapse is a phenomenon that occurs with the interaction between the fuel plumes of a multi-hole injector, for determinate physical conditions.

For multi-hole GDI sprays, spray collapse can happen both at non-flash boiling, and flash boiling condition. Guo et al.[25] explained them as jet induced collapse and condensation induced collapse, respectively. In both cases, the interaction between the spray plumes is the precedent phenomenon which can be considered the cause of the collapse. In the two following sections, it is explained deeper the developing of the two kind of collapse and which factors this phenomenon depends on.

#### 4.3.1 Jet-induced spray collapse at elevated ambient pressures

During the injection, the air inside the spray plumes is accelerated due to the momentum exchange: air loses static pressure and gains velocity, exchanging momentum with the fuel flow.

As the local static pressure decreases, in the surround of the multiple jets a gap of pressure is created (low-pressure core).

In the zone under the nozzle tip, where the gap is significant, the surrounding gas is sucked into the jets, factually

balancing the low-pressure zone. This is true when the density is low enough to allow the external gas to enter the low-pressure zone, being the spray plumes narrow to leave an entrance for the gas (*Figure 4.4*).

As the ambient pressure increased, the spray plumes would become wider and resultantly the gap between the jets (entrance for the external gas) would become narrower, preventing the external gas from entering the enclosed low-pressure zone. In this situation, the plumes are sucked inwards, instead of the chamber gas. The difference between the two situations is highlighted in the footprints of *Figure 4.4*.

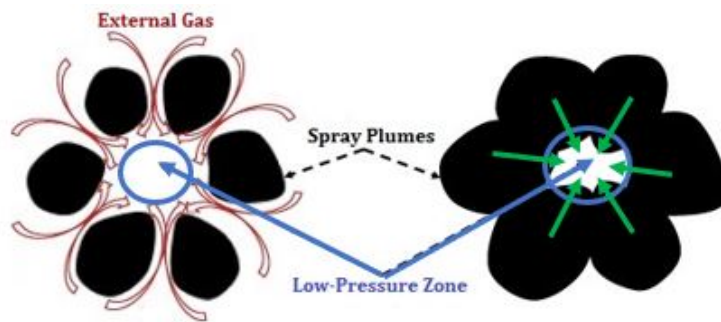


*Figure 4.4: Different air motion between non-collapsed (left-hand side) and collapsed (right-hand side) spray*

However, in the far field of the spray, the low-pressure core is greatly weakened. Firstly, the air inside the jets is slower due to the deceleration of the fuel flow. Secondly, the density of the droplets is much lower than that in the near field.

In conclusion, it is possible to state that, at elevated chamber pressure, spray collapse will occur mostly in the near field of the spray, without vaporization of the fuel flow (non-flash boiling conditions). It is attributed to the generation of low-pressure zone caused by the shape of the surrounding high-speed jets: for this reason, the phenomenon is called jet-induced spray collapse. It depends on chamber density.

### 4.3.2 Condensation-induced spray collapse under flash boiling conditions

As it has been stated in [25], the spray collapse phenomenon is not only detected in the near field of the injection, but also in the far field. Therefore, there must be other factors leading to the spray collapse which occurs in the far field. Indeed, it can be associated to the flash boiling condition: it is believed that vapor condensation is the primary cause of spray collapse under flash boiling conditions (*Figure 4.5*).

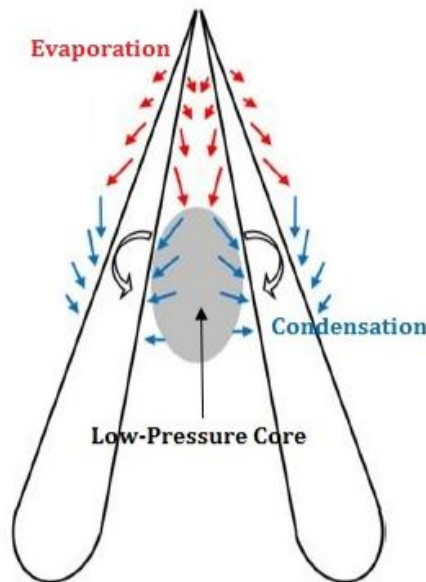


*Figure 4.5: Mechanisms of the condensation-induced spray collapse [25]*

The vapor condensation is the result of the vapor temperature drop, due to the vapor expansion work, during the bubble growth phase of the flash boiling phenomenon. This is the so-called Joule-Thomson effect, also known as “auto refrigeration”. When a gas expands, like in the bubble growth phase, the average distance between its molecules increases. Given the presence of intermolecular attractive forces, expan-

sion causes an increase in the gas potential energy. If work is not extracted from the system during the expansion process ("free expansion") and no heat is transferred (adiabatic expansion), total gas energy remains the same, due to energy conservation law. The increase in potential energy therefore produces a decrease in the kinetic energy and therefore a decrease in gas temperature.

Hence, due to the drastic temperature drop, the vapor in the surrounding of the spray can be condensed in the form of mist or taking the low temperature droplets as the nucleus. The disappearance of massive vapor leads to a violent pressure reduction inside the spray field, creating a low-pressure core. It means that the spray plumes will be sucked inwards by the surrounding gas, which tries to enter in the low-pressure zone, leading to the spray collapse.

The effect of the temperature drop and the resultant condensation have been deeply explained in [25], while in other previous studies on the flash boiling spray collapse, they have not been highlighted. For this reason, further investigations are needed, for a total understanding of the effects of condensation process on the collapse. Anyway, it would be enough to explain the collapse caused by the flash boiling process just with the evaporation of the liquid spray. Indeed, evaporation creates wider spray plumes, which, interacting each other, as previously seen, lead to the spray collapse.

In conclusion, the far-field collapse under flash boiling conditions is attributed to the generation of low-pressure zone caused by temperature drop (with resultant vapor condensation) and by the evaporation process. It occurs with the same conditions of the flash boiling: superheated fuels and sub-atmospheric cylinder pressure.

## Chapter 5

# Experimental Equipment

In this section, an overview of the required experimental equipment is given. Within the facilities of CMT – *Motores Térmicos* and *Universitat Politècnica de València*, it has been necessary to prepare and arrange all the equipment in the laboratory, in order to carry out experimental tests. The project consists in developing a methodology to characterize the spray for a multi-hole injector, in order to simulate the process of complete injection for GDI applications, from the transient flow of the nozzle to the formation and development of spray under non-reactive conditions.

### 5.1 Test rig

In order to carry out the experimental part of this project, in the CMT centre, a test rig has been built which serves as test chamber (*Figure 5.1*). The prototype has the shape of a tetrahedron, with constant volume, entirely manufactured in AISI 1020 blued steel, whose main characteristics can be found in the table *Appendix ??* [27]. The bluing (or blue tempering) is a process of heat treating, carried out by polishing the steel and heating it between 290 and 310 °C: the effect of this process is to create a dark blue layer of  $\text{Fe}_3\text{O}_4$  around the parts to prevent the corrosion and improve their

appearance. On the lateral surface, the prototype presents four circular openings on which windows have been mounted to allow the optical investigations. Furthermore, one of the lateral windows has been realized purposely to allow the entrance of the injector and, consequently, is different from the others (*Figure 5.1*). The openings on the top, instead, constitute the entrance and the exit for the air and the enclosure for temperature and pressure sensors.

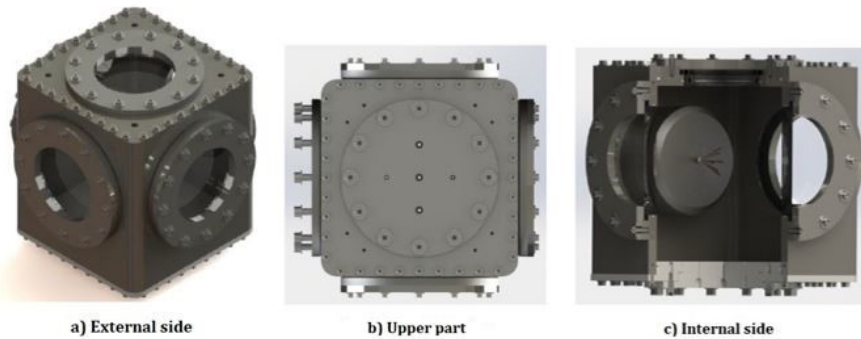


**Figure 5.1:** Representation of the test rig: external side (a), upper side (b), internal side (c) [27]



**Figure 5.2:** Opening for the resistance from the inside (a), from the outside (b) and cylinder casing of the resistance (c)

Finally, at the bottom, another window has been built to allow the resistance insertion, in order to regulate the temperature of the air within the chamber (*Figure 5.2*). A casing built in the same material of the test rig is responsible

to contain the resistance and to assure the heat insulation. The resistance has been inserted and fixed within the casing in such a manner to be sure that cannot touch the walls of the casing all along its length.

The test chamber is strong enough to reach all the pressures from 0.2 to 15 bars, as a result of the large number of screws in the windows and the use of O-rings, as the sealing between the crystal windows and the test rig is paramount (*Figure 5.3*). The resistance allows to reach temperatures within the chamber from ambiental to 120 °C.

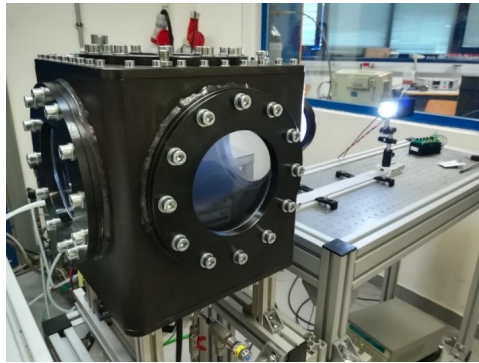


*Figure 5.3: Test rig arranged for the tests with screws and O-ring clearly visible*

## 5.2 Injection system

This section presents the geometry of the injector used for the tests. The real innovation is that the study is carried out with a new model of piezo-injector developed by DENSO Corporation. The injector has been tested in a wide range of conditions capturing both the liquid and vapor phase of the spray. DENSO company failed to submit any information in respect of the internal geometry and the characteristics of this kind of injector. Nevertheless, in *Figure 5.4*, the exterior

geometry of injector is represented as clearly as possible.



*Figure 5.4: External geometry of the injector (CMT)*

The injector presents six symmetrical orifices, as it is shown in the plant of *Figure 5.5*, without the proportions in the measurements being respected. The camera with which all the measurements have been taken is positioned on the symmetry axis, so as to preserve the symmetry of the orifices. Finally, *Figure 5.5* is a zooming of the nozzle tip.

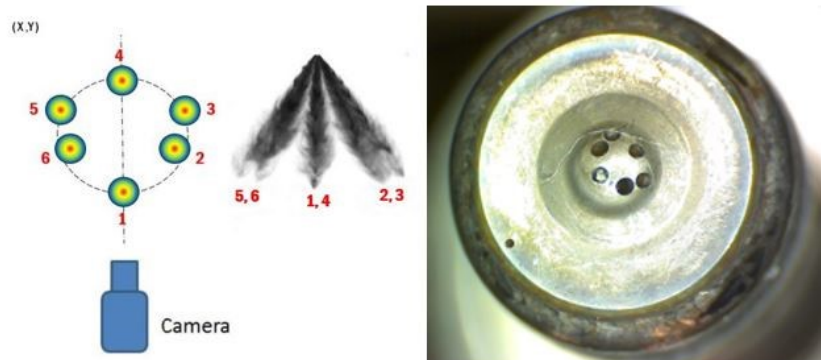


*Figure 5.5: Plant of the position of orifices (left) and zooming of the nozzle tip (right)*

The injector has been connected to an electronic power

unit powered by an electric generator. The injector logic control unit is a TTL (Transistor-Transistor Logic) four channel digital delay/pulse generator, which is shown in *Figure 5.6*. The injector has been inserted in the test rig from the lateral window specially designed for it, in a way that allowed the optical analysis through the other two adjacent lateral windows, as indicated in *Figure 5.6*.



*Figure 5.6: Logic control unit (left) and internal view of the test rig with the position of the injector outlined (right)*

In the *Table 5.1*, other important specifications of the injector are gathered, for the purposes of information. It should be noted that the temperature of the nozzle, hence of the orifices, is held constant at a value of 90 °C.

<b><i>Parameter</i></b>	<b><i>Specification Value</i></b>
<i>Number of holes</i>	6
<i>Orifice diameter</i>	220 $\mu\text{m}$
<i>Hole shape</i>	straight
<i>Spray shape</i>	circular
<i>Temperature nozzle</i>	90 °C
<i>Injector frequency</i>	0.25 Hz

*Table 5.1: Other specifications of the injector*

### 5.3 Fuel used

Gasolines are formed by different types of hydrocarbons and their distinction is a function of the different elements that contribute to form them. Fuels used throughout the testing phase of this work are components of commercial gasoline. In descending order of their number of carbon atoms, the tested fuels are iso-octane ( $C_8H_{18}$ ) and n-heptane ( $C_7H_{16}$ ).

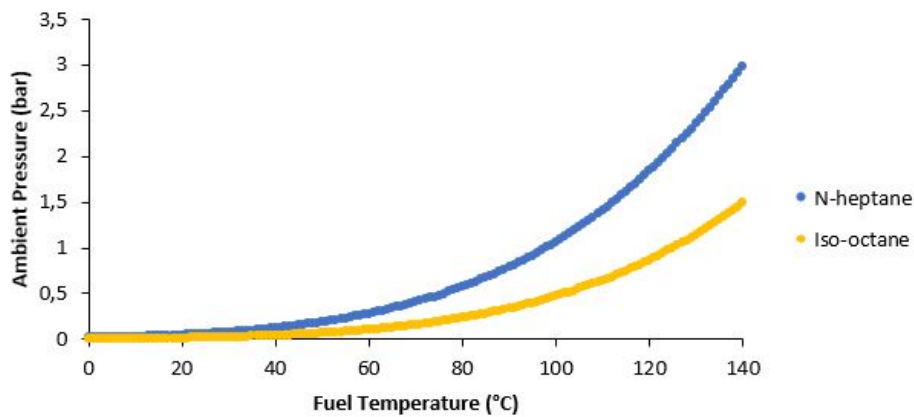


*Figure 5.7: Saturation curves of the tested fuels*

In *Figure 5.7* the difference in their volatility is visible, due to the representation of their saturation pressure curve. The data for the saturated pressure against liquid temperature was obtained from the National Institute of Standards and Technology (NIST).

Iso-octane has the lowest curve of saturation pressure: it means that, with iso-octane, flash boiling process is less likely to appear. N-heptane is very important for the results of the test because it represents a benchmark for ECN group results, allowing also other partners of the collaborations to have a comparison in further researches. Furthermore, it is used to determine the octane number of a gasoline. Using

both the components in the tests, it will be evident the effect of the volatility on the spray behaviour. Of course, the difference will not be considerable, due to the close properties of the components. Either way, it will be enough to be noticed with the optical apparatus employed.

At the beginning, it has been thought to use also the hexane, which possesses much higher volatility and hence more chance to evaporate, under the same thermodynamic conditions (as shown in the *Appendix ??*). Unfortunately, after an accurate evaluation, it has not been possible to use it, due to security issues. As outlined in the graph of *Appendix ??*, hexane possesses also nearly the same trend of saturation pressure of the European commercial gasoline.

#### 5.4 Optical set-up

The acquisition of images has been done using either Diffuse Back-Illuminated (DBI) imaging and Single-Pass Schlieren Shadowgraph method. The field of view of both these two methods is a lateral view of the injection nozzle.

The technique Diffuse Back Illuminated (DBI) imaging has become the standard for liquid length measurements in the ECN organisation. Particularly, it exploits the light refraction gradients to measure the penetration, angles and volume of the spray liquid particles; hence, the vapor in the chamber is not visible with the technique. Conversely, the Schlieren process is used to characterize the liquid and vapor penetration of the spray, through density gradients.

The details for each optical subsystem are explained deeper in the following subsections.

#### 5.4.1 Single-Pass Schlieren technique

The Schlieren photography was invented by the German physicist August Toepler in 1864 during his research on the supersonic regime. It is a method widely used to characterize the flow of fluids of varying density, mostly in the aerospace field. It exploits the difference of the air density and can be used to characterize the physic phase of the fluid.

The compression applied on the fluids changes their density and therefore also their optical properties (refractive index), namely the way they interact with the light that passes through them. Even a heat source can cause variations in the density of the fluid in which it is immersed. It suffices to think of the air between our eyes and a campfire for example, or the surface of very hot objects, such as asphalt: they seem to be flickering and they can cause a visual deformation because of the changes in their density.

In this case, Schlieren imaging has been used to differentiate the vapor phase of the spray from the ambient gas of the chamber: indeed, it is discovered to be a valid method for the measurements of angle and penetration of the vapor phase of the spray. Because of the characteristics of a GDi injector, the developed spray angle is very small ( $80^\circ$ ) compared to the Diesel case ( $150^\circ$ ), resulting in the spray moving forward more than sideways. Mostly for this reason, it makes sense to use the lateral view more than the frontal one, to characterize the morphology of the spray [26].

The fundamental principle behind Schlieren optical systems is that light rays travel in space or transparent media in straight lines unless their direction is altered by some obstacle. Interferometric systems usually depend on a phase shift associated with changes in the velocity of light.

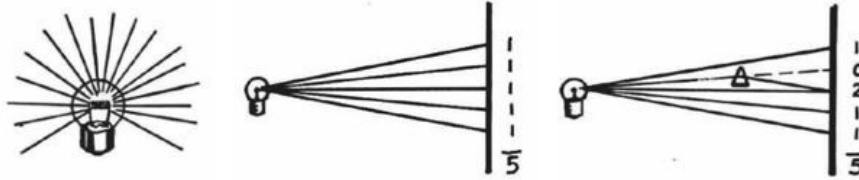


*Figure 5.8: Schlieren functioning principle. From left to right: light source, undisturbed light pulses, altered path light [28]*

Firstly, a light source is required. For now, the considered source is a “point” source, thus, at least in theory, emanating light pulses uniformly in all the directions (*Figure 5.8*). When light from this source falls on a screen, the screen will appear to be lit up by the light rays falling on it. If the source is enough far away from the screen, then the change in distance between the source and the edges of the screen will be negligible. This will result in an energy distribution which is shown in *Figure 5.8*. It means, namely, there will be the same units of energy per unit surface area. Simply, it can be said that on any given spot there is one light ray falling. In the drawing, over the five points schematically shown, it is measured one ray for each point, with five total units of light energy. However, if something is put between the light and the screen, the previously situation will be disturbed and the light path will be altered. It can be noted, in *Figure 5.8*, that from one place the light has been removed, with the illumination falling to zero and at another place, the light that was taken from the previous point is added to that point with the consequence that the illumination is doubled. This area appears twice as bright as the undisturbed surround. Anyway, the total energy has remained unchanged. This is the principle on which depends the functioning of the Schlieren imaging.

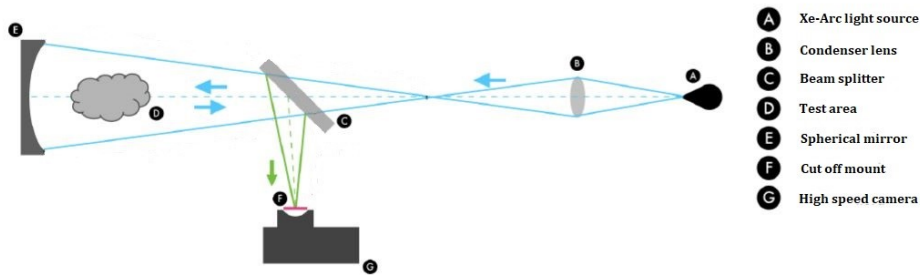


*Figure 5.9: Single-mirror Schlieren setup design [29]*

The system was assembled in the laboratory firstly arranging components as shown in *Figure 5.9*, and then accurately calibrating the positioning of the equipment for optimum results. The optical path, as aforementioned, starts with the light source produced by a continuous Xe-Arc lamp connected to a fibre optic. After that, the light pulses pass through a condenser lens. A condenser is a screen which renders a divergent beam from a point source into a parallel or converging beam to illuminate an object. Condensers are an essential part of any imaging device, in order to obtain a uniform distribution of the light pulses. Afterwards, the light pass through a beam splitter prism to get better alignment. Now the light pulses are ready to pass through the object to look at (in this case, the spray). Behind the examined object, a spherical concave mirror is placed, with a long focal length. The value of the focal length is essential to take in consideration, because the light source must be placed exactly two times the focus length away from the mirror surface. Finally, it is necessary an optical system, in this case a high-speed camera, placed behind a cut-off mount, in order to block the refracted light pulses. In this case, what has been used is a circular pattern cutting device, as it cuts the deviated light in a symmetrical manner. The cutting device is a crucial part of the equipment since it constitutes the control of the

sensitivity of the experiment. Right after the cut-off mount, an high-speed camera captures the images formed in the set-up, which will be composed of black zones and clearer zones: the dark zones will represent the light that has been deviated by the spray and discarded in the cut-off device, while the clearer zones will represent the background of the images where the light has not been deviated.

#### 5.4.2 DBI technique

Diffuse-Back Illumination technique was used to measure liquid penetration and liquid spray angle thanks to the refraction of the light pulses. The scheme of a general DBI measurement system is represented in *Figure 5.10*. It is mainly composed of a high-speed camera, an emitter of light, a Fresnel lens, a diffuser.

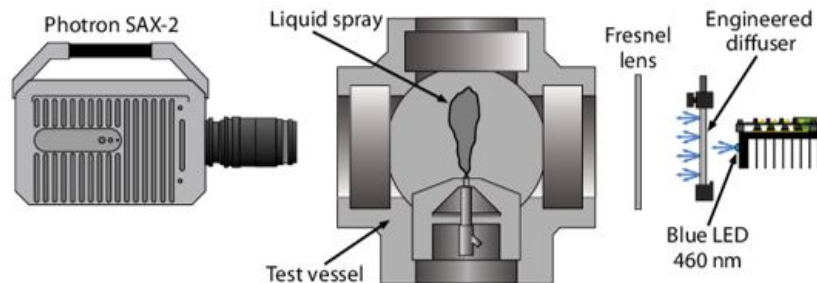


*Figure 5.10: DBI optical system setup [30]*

As it is easily visible in *Figure 5.11*, it has been faithfully respected also in the laboratory for the experimental analysis. The high-speed camera used for the tests is a *Photron* with a framerate of 35000 fps. The pulse of light is emitted by an ultra-fast blue LED. The light then passes firstly through a diffuser, and secondly through a lens, to obtain a diffused light wide enough to cover the complete test area

(*Figure 5.12*). Once the pulses of the light reach the chamber and, consequently, the spray, three situations are possible:

1. The light which encounters in its path the sprayed fuel in the liquid phase will be blocked. The high-speed camera, on the other side of the chamber, will detect a black zone, which will be visible obviously also on the recorded videos.
2. The light which encounters the vapor phase of the spray will be slightly deviated and attenuated. For this reason, on the recorded videos, these zones will appear grey or, either way, attenuated.
3. The light which encounters just the ambient gas (not the spray) will be undisturbed. The corresponding zone on the recorded videos by the camera will appear white, because of the undisturbed light.

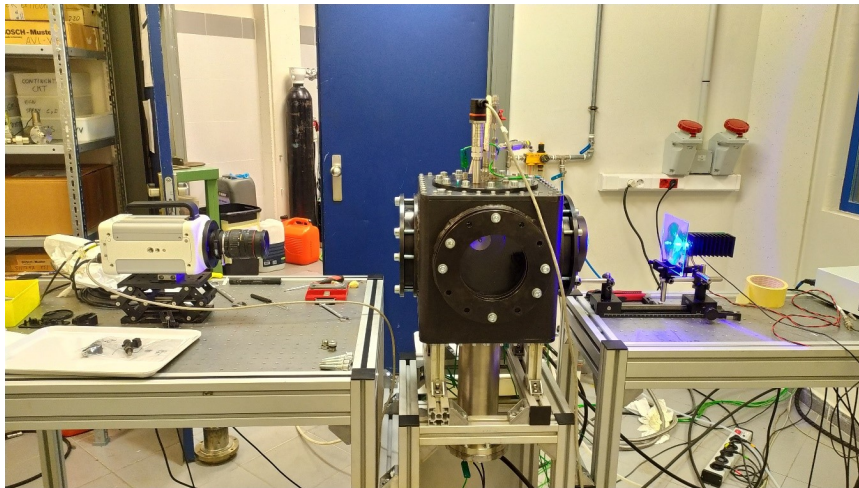


*Figure 5.11: DBI equipment arranged for the tests (CMT)*

In the case of DBI, the pulses of the light are not parallel, because of the diffuser. This is the reason why a cut-off device in front of the camera is not necessary in the DBI case, unlike

the Schlieren technique. Anyway, even if it seems evident that also with DBI it should be possible to visualize correctly the vapor phase in the measurements, this is not completely true: indeed, the grey and white zones do not possess enough contrast, in most cases, to be correctly distinguished by the processing algorithms.

In conclusion, the images captured with this measurement system are basically dark in correspondence of liquid phase and white or light grey in correspondence of background and vapor phase.

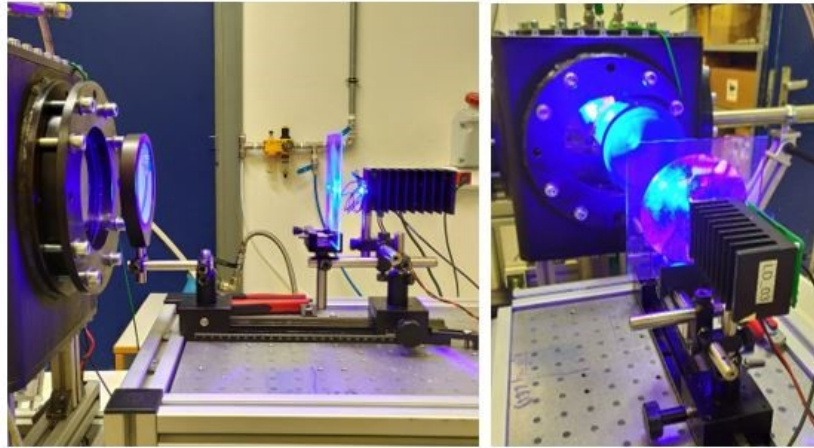


*Figure 5.12: Focus on the light source, diffuser and lens used for the tests (CMT)*

## 5.5 Test matrix

The experimental conditions selected ranged from  $1.3 \text{ kg/m}^3$  to  $12.2 \text{ kg/m}^3$  of gas density within the combustion chamber, with the injection pressure varied between 100, 200 and 280 bars. The fuel temperature fixed to  $90 \text{ }^\circ\text{C}$ . Actually, the changes in ambient gas density has been carried out by varying two parameters, which are the ambient pressure and the

ambient temperature of the combustion chamber. Nevertheless, in the graphs, it was decided to visualize the gradients of ambient density, to have just one factor of comparison to characterize the great amount of collected data. Indeed, due to the ideal gas laws, density directly depends on temperature and pressure, as follows:

$$\rho \sim \frac{p}{T} \quad (5.1)$$

The tests have been carried out also with two different values of energizing times: 680 and 1500  $\mu\text{s}$ . By way of conclusion, *Table 5.2* shows a summary of all the specific conditions measured in the tests.

<b>Parameter</b>	<b>Values</b>
<i>Ambient Gas Density [kg/m<sup>3</sup>]</i>	<i>1,3 - 1,8 - 2,5 - 3,5 - 4,2 - 5 - 5,9 - 7 - 8,8 - 12,2</i>
<i>Ambient Gas Temperature [K]</i>	<i>573 - 800</i>
<i>Ambient Gas Pressure [bar]</i>	<i>3 - 6 - 8 - 10 - 12 - 21</i>
<i>Injection Pressure [bar]</i>	<i>100 - 200 - 280</i>
<i>Injection Temperature [K]</i>	<i>363,15</i>
<i>Energizing Time [<math>\mu\text{s}</math>]</i>	<i>680 - 1500</i>
<i>Fuels used</i>	<i>Iso-octane, N-heptane</i>
<i>N° repetitions / condition</i>	<i>10</i>

□

**Table 5.2:** *Test Matrix*

## Chapter 6

# Experimental Techniques

### 6.1 Introduction to the experimental strategy

In order to achieve the objectives, the path has been divided in different steps, which are represented in *Figure 6.1* , in a chronological order.

Firstly, all the apparatus has been prepared for the experiments: the assembly of the missing parts for the construction of the test chamber was finalized, the thermo regulator of the oil for the injector jacket has been modified for the needs of the experiment, the necessary quantities of fuel have been ordered. Once everything was ready for the measurements, the test process started. Afterwards, the next step was the image processing, in which all the obtained images were processed with MATLAB In-House algorithms, appropriately modified and calibrated for this work. Finally, the obtained results were analysed to draw conclusions.

Hereunder, the image processing system has been explained deeper, in order to a better understanding of the results, due

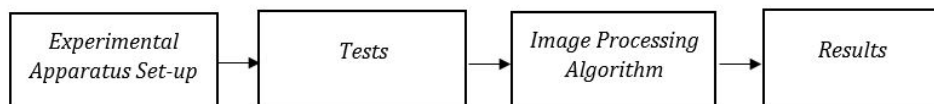


*Figure 6.1: Steps of the testing process*

to the difficulties encountered to make them reliable and precise.

## 6.2 Image processing system

The phase of image processing is essential for the correct visualization and subsequent analysis of gathered data. The processing of the images, as already explained previously, has been done with developed algorithms in which all the images, regardless of the optic technique used to take them, were combined to be processed in the same way. Hence, given the difference in the images obtained, a pre-processing algorithm was used to adapt the distinct type of pictures.

First, it was necessary to relate the configuration of the camera to the programme for the processing of the images. In order to do this, a configuration file was created, within which all the camera settings are stored. Afterwards, the geometry of the captured images must be set up. It means to indicate to the programme as input all the geometrical data and the relation between pixel per millimetre. Here, the programme will know the nozzle position, the spray exit, the start of the detection of the spray, the end of the detection and the numbers of spray tested in the optical window, as shown in *Figure 6.2*.

The next step is to detect the contour of the sprays. The detection of the spray contours must be as precise as possible, to assure the reliability of the final results. The methodology to find the spray contour is not unique, given that a clear distinction between spray particles and lit background is impossible to obtain.

What is essential is, once identified the best parameters and to characterize the spray contours, to always keep them fixed for all tests of the investigation. Only in this way, at

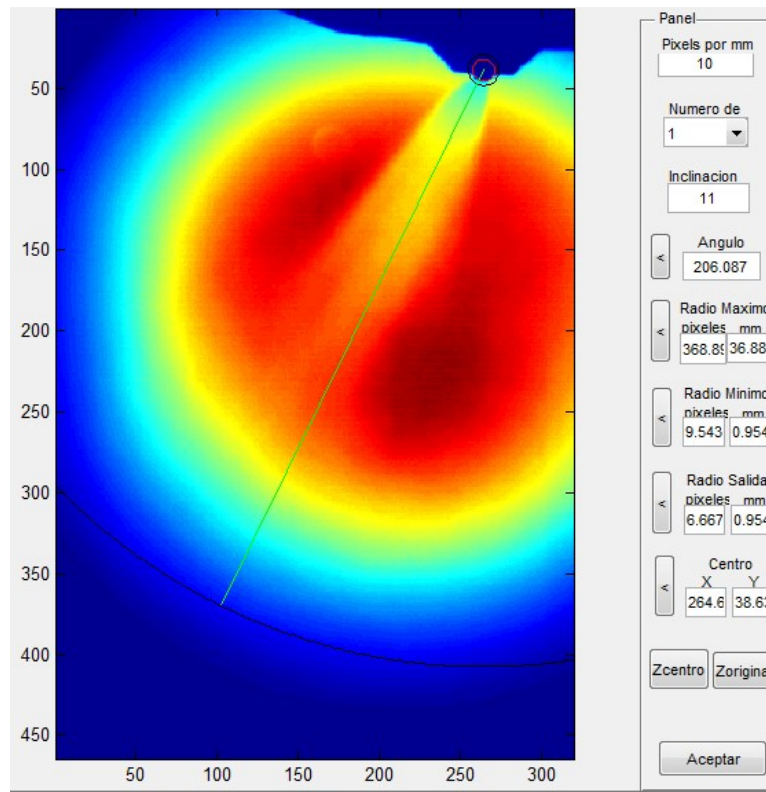


*Figure 6.2: Set-up of the geometry of the images*

the end, it is possible to compare the obtained results.

In order to detect the contour of the spray, the first step is the background subtraction. The process to perform it is different, depending on the technique utilized. In the DBI technique, the background is static. For this case, a simple average of the first 8 images is enough to prepare the background to extract. In the Schlieren technique, the density gradients are visible, hence the movement of ambient gas in the background is noticeable: here the background is dynamic and it is different for every image. Everything that is not detected as spray is taken and put in the same place in the current image. The, the part of the previous image where the sprays where detected is taken and filled with the corresponding positions of the background generated with the

average of the first 8 images.

Afterwards, it is necessary to perform a binarization, creating a black and white binary image, where the white colour represents the detected spray particles and the black is the rest. A threshold is essential to be determined in order to create the binary image. The threshold is a luminosity intensity value that represents the difference between spray and background. However, the resulting binary images could be not perfectly representative because some zones in the background can appear more illuminated: hence, cleaning is necessary and a binary erosion filter must be applied. Once the erosion is performed, the images can be passed to the processing code, in order to detect the contours, taking in consideration the threshold previously set by the user.

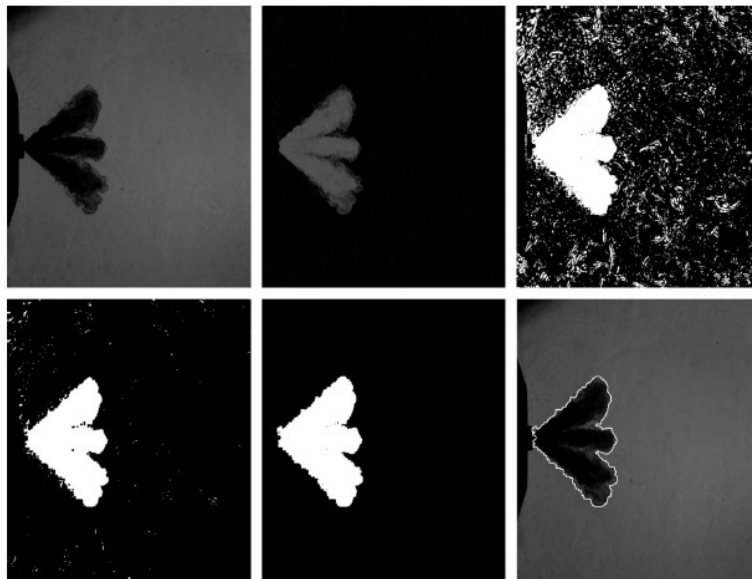


*Figure 6.3: Example of the image processing for a Schlieren image [26]*

*Figure 6.3* well characterizes the steps described: top left represents the original image, top centre shows the subtrac-

tion of the background, top right is the result of the binarization, bottom left presents the erosion filter applied, bottom centre the image with the contours ready to be detected, bottom right the image with the contours overlapped.

### 6.3 Contour processing

Once that all the images have been processed and the contours of the spray (vapor and liquid particles) have been detected, the two main results that have to be extracted from the experiments are penetration and spray angle.

The penetration has been extracted from either vapor and liquid phase, with good precision, through an average value calculated over the 10 injection repetitions tested, for each condition. In *Figure 6.4* is shown, by way of example, a raw image ready to be post-processed, captured at a certain value of time ASOI: in red the contour of the liquid (left-hand side) and of the vapor (right-hand side) phase, in blue the furthest point to the nozzle from which is measured the penetration.

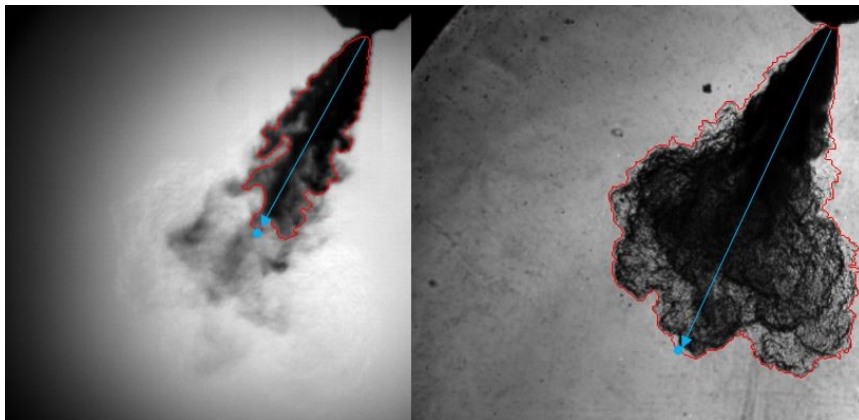


*Figure 6.4:* Raw image which highlights liquid (left) and vapor (right) contour of the spray (red) and penetration (blue)

The spray angle is a more difficult measurement to de-

termine, given the complexity of extracting representative results due to the high dependence on definition used.

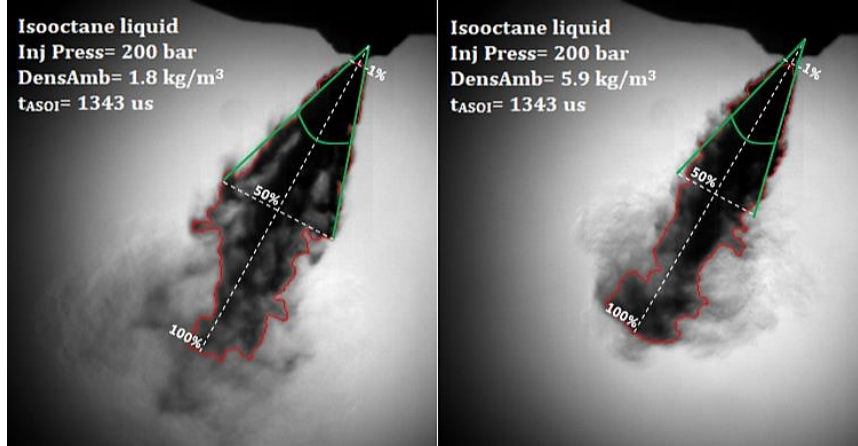


*Figure 6.5: Raw images in which the characterization of the liquid spray angle is marked, for different densities*

For the case of liquid phase captured with DBI method, the main source of uncertainty is that, as it can be seen in *Figure 6.5*, the contour of the spray (also after the average among the 10 repetitions) is not completely triangular and the lines can be rounded. Hence, the angle has been calculated carrying out a least square fit with the lower and upper parts of the contour. Considering the *Figure 6.5*, it can be noted the huge difference between the shape composed by the contour of the two cases. On the left-hand side image, where density and temperature are lower, the outer shape can be approximated with a triangle, while on the right-hand image the overall shape is more irregular, due to the different physical conditions of the chamber. This creates the necessity to set limits of the contour used for the fit, for each time window in which the spray angle is measured. After considerations, the choice fell on setting two penetration limits, of which the first one very close to the nozzle (in order to avoid

parallel lines if the first part of the spray is disregarded) and the second one not very far, to avoid the turbulences and the irregularity formed due to the long-time ASOI. After a lot of attempts, the limits were fixed at 1% and 50% of the axial spray penetration, also accordingly to other experiments carried out, i.e [26].

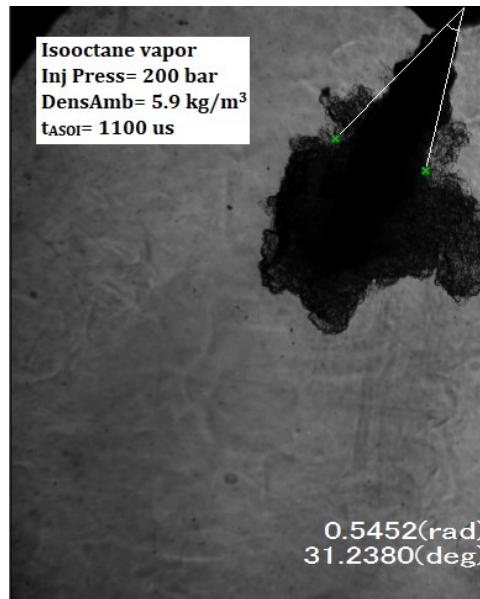


*Figure 6.6: Raw Schlieren image*

For the vapor case, instead, as it can be seen in *Figure 6.6*, when the spray is characterized by a higher value of density, the model to calculate the spray angle described up here loses its meaning. Indeed, this image presents a thin spray cone in the beginning, close to the nozzle, but then it rapidly expands to an oval shaped contour, rendering the measurement meaningless. This phenomenon can also occur at lower density and makes incompatible all of the definition tried. Given that the importance of the angle measurement is mainly the understanding of the spray collapse phenomenon, which is not a phenomenon related to the vapor phase, considering

the incompatibility with the model used for the liquid spray, it has been decided to not characterize the vapor spray in terms of spray angles.

## Chapter 7

# Results

After the algorithms of image processing, the detected contours of the spray are ready to pass to the post-processing codes to extract the results. The interesting results extracted from the tests concern penetration and spray angle. In the following sections, given the large amount of processed data, only the most significant graphs resulting from the experiments are reported. The others, which are necessary to assure the validity and reliability of the results, can be found in the *Appendices*. To guarantee the consistency of the results, ten repeated tests were conducted under each experiment condition: in conclusion, each line plotted in the graphs has been obtained by the average of ten measurements under the same experimental condition.

### 7.1 Penetration

The penetration is extracted, for each time window, selecting the furthest point of the spray contour, considering only the axial distance to the nozzle. The algorithm to calculate the penetration is not particularly complicated, once it is known the spray contour: it is enough to extract the penetration value from the point whose distance from the nozzle is the longest one, for each fixed time interval.

### 7.1.1 Effect of gas density variation

Throughout the work of the engine, several gas-density values may be achieved inside the combustion chamber and the injector should be able to supply the proper quantity of fuel at all of these possible conditions. Like for the Diesel ones, also the GDi injectors have a clear relation between gas density and penetration: for this reason, the ambient density is one of the most influential parameters for the characterization of the spray.

*Figure 7.1* shows vapor and liquid penetration results for the range of densities analysed, both with ambient temperature of 573 K (top) and 800 K (bottom). Hence, to vary the density for this particular case, the ambient pressure changed. The density in the first figure ranged from approximately the same values as for the second one. The injection pressure for this case was maintained fixed at 200 bar. These graphs are useful to demonstrate that both vapor (dashed lines) and liquid (solid lines) penetration of iso-octane decrease with increasing ambient density of the combustion chamber. This is due to the fact that, with the increasing of ambient density, pressure in the chamber raises (bearing in mind that the chamber temperature is fixed at a determined value) and the fuel particles exiting from the injector nozzle encounter more rolling air resistance.

The trends of liquid and vapor penetration in the first picture are the ones expected and reported several times in the Diesel spray literature [31]. Indeed, in this case, the ambient temperature of 573 K is not high enough for the gasoline to evaporate till the point to lead to the stabilization of the liquid penetration.

On the other hand, analysing the second graph, it can be appreciated the stabilization of the liquid penetration, due

to the major ambient temperature which leads to a stronger evaporation phenomenon. As it is visible in the graph, evaporation occurs at the same spray length for all the density conditions tested: it means that, in the evaporation mechanism, the density condition is negligible compared to the temperature of the fluid. As a confirmation of this, said stabilization can be seen from around  $1500 \mu\text{s}$  after the start of injection (ASOI) for all the density conditions tested.

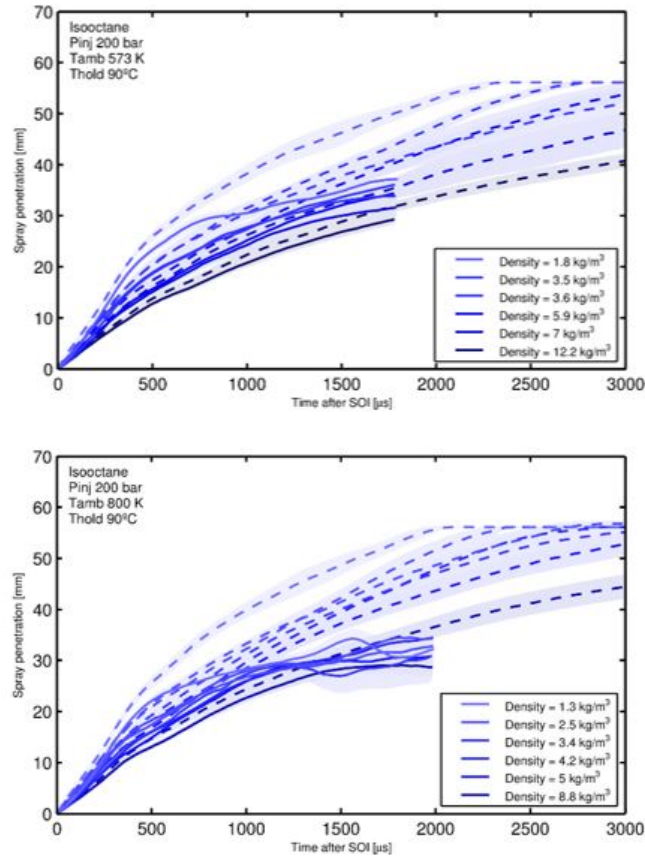


**Figure 7.1:** Density variations for 573 K (top) and 800 K (bottom), for vapor and liquid penetration

In *Figure 7.2* and *Figure 7.3*, some raw images, among the most representative ones, are shown, where the difference in ambient density is appreciable: on the left-hand side the

spray is injected in a chamber with a density value of  $1.8 \text{ kg/m}^3$ , while on the right-hand side the ambient density is fixed to  $12.2 \text{ kg/m}^3$ . The difference of densities is visible, in the backgrounds of Schlieren measurements, also to the human eye.

It is visible, either in the DBI and Schlieren penetrations that, with higher density, the spray plume is shorter, for each given time ASOI. Obviously, the behaviour of the spray shown in the raw images perfectly follows the trend of *Figure 7.1*, given that the red detected contour has been processed to plot the represented graphs.

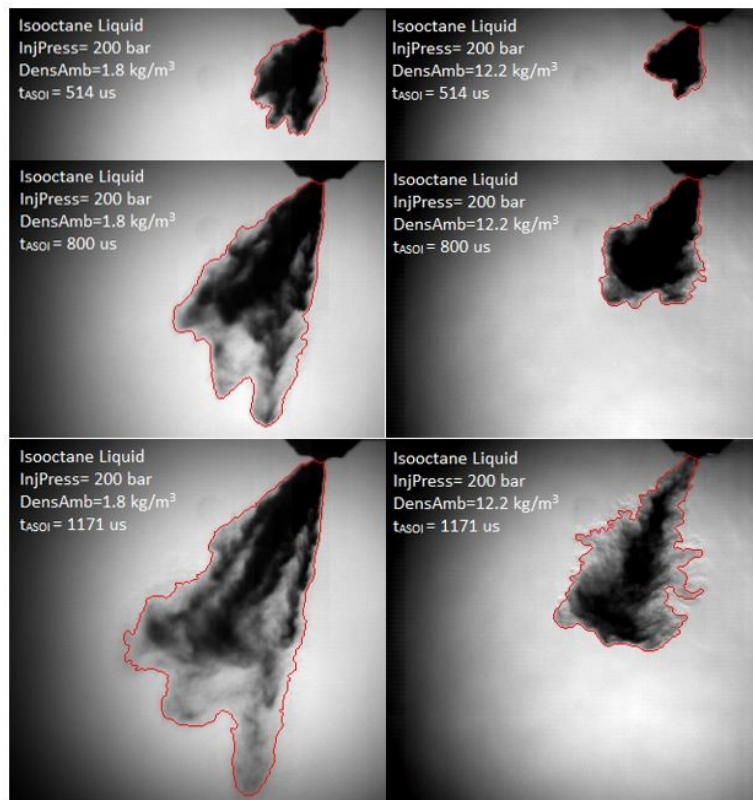


**Figure 7.2:** Liquid spray comparison between lower density conditions (left) and higher density conditions (right) using raw images and the detected contours

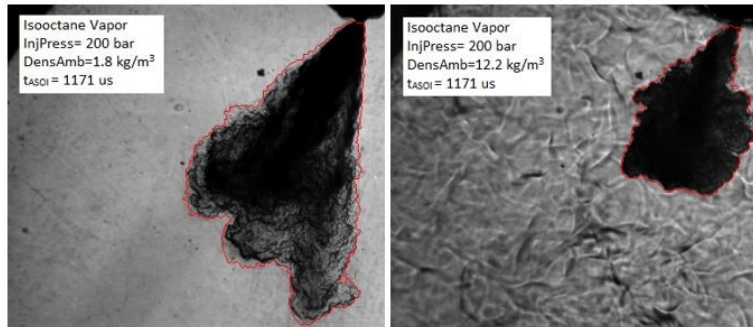


**Figure 7.3:** Vapor spray comparison between lower density conditions (left) and higher density conditions (right) using raw images and the detected contours

### 7.1.2 Effect of the injection pressure

During the operation of the engine, the variation of injection pressure is another key parameter worth analysing, given that it could affect the behaviour of penetration and spray angle.

Three injection pressure values (100, 200, 280 bar) have been tested for all the possibilities of other conditions.

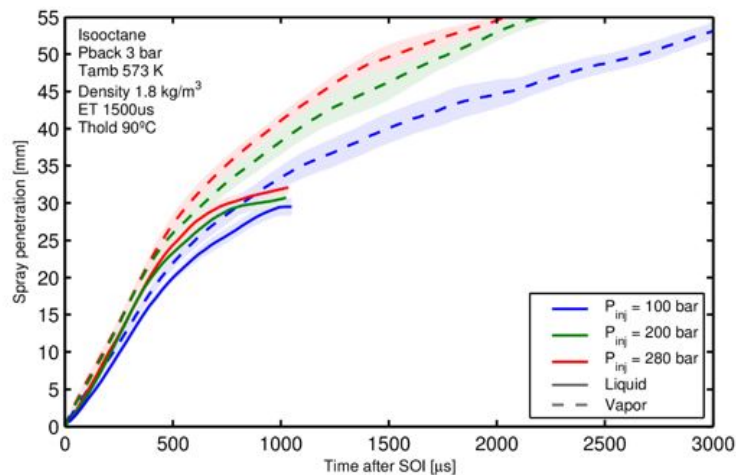


**Figure 7.4:** Injection pressure variations for iso-octane vapor and liquid penetrations

Beginning with iso-octane tests, *Figure 7.4* shows the ef-

fect of injection pressure on the liquid and vapor penetration, for a low ambient density condition of  $1.8 \text{ kg/m}^3$ . Considering the vapor curves, it is visible that, as the injection pressure increases, the vapor spray penetration is augmented. However, the liquid penetration is not greatly affected. This agrees with Diesel literature. The reason is that, by increasing the injection pressure, according to the conservation law, causes the momentum of the fuel to grow. This is reflected in a growth of the penetration, mostly for the vapor one, given that the liquid particles at a certain point (not depending on the injection conditions but rather on the ambient ones) begin to evaporate. Hence, when the liquid particles begin the evaporating and enter the vapor phase, they continue to behave as they did throughout at the liquid stage.

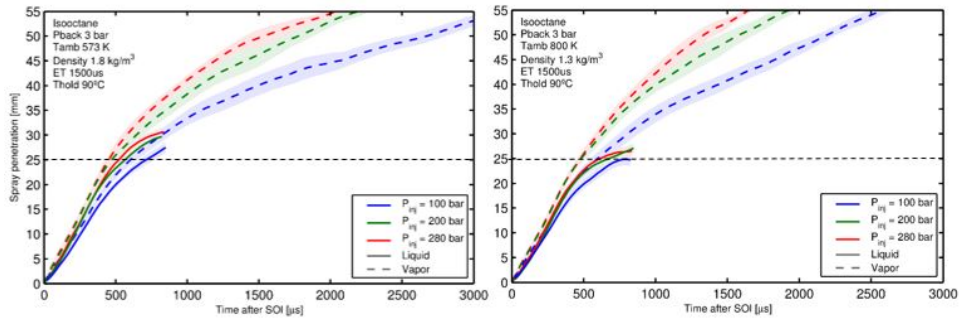


**Figure 7.5:** Injection pressure variations for two different back temperature values: 573 K (left) and 800 K (right)

The next step is to analyse how the aforementioned behaviour of the spray is affected by the increasing of the only temperature within the chamber, varying the injection pressure. *Figure 7.5* shows two graphs, in which the temperature has been varied from 537 K (left-hand side) to 800 K (right-hand side). Considering the liquid penetration, it is visible that, with major ambient temperature, the evaporation phenomenon is anticipated. The effect in the graphs is not very

evident because of the slight drop of temperature tested.

In conclusion, with regard to the injection pressure variation, the plots presented show that it is not a very influent parameter on the liquid penetration of the spray plume, while it has a stronger impact on the vapor penetration, as a consequence of the evaporation phenomenon: indeed, vapor penetration is higher with increased injection pressure and continuously increases with time, as stated also in [31].

### 7.1.3 Effect of the type of fuel used

The graphs represented in *Figure 7.6* allow direct visualization and comparison of liquid and vapor penetration between iso-octane and n-heptane, by varying the injection pressure. In order to facilitate the visualization, the intermediate pressure injection curves (200 bar) have been removed, as the trend is sufficiently evident with two pressure curves.

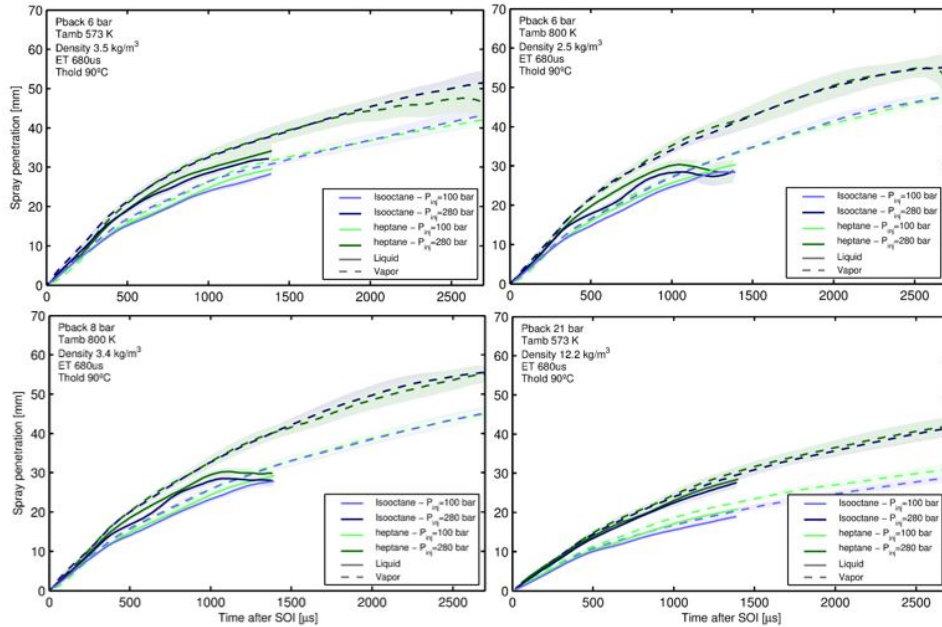


*Figure 7.6: Effect of fuel properties on the spray penetration, under several conditions*

For a full understanding of penetration trends, representative properties of the tested fuel in *Table 7.1* should be carefully analysed.

<b>Fuel</b>	<b>Liquid Density (kg/m<sup>3</sup>)</b>	<b>Dynamic Viscosity (mPa/s)</b>	<b>Kinematic Viscosity (mm<sup>2</sup>/s)</b>	<b>Surface Tension (mN/m)</b>
<i>N-heptane</i>	684	0.376	0.55	20.14
<i>Iso-octane</i>	689	0.456	0.66	18.77

*Table 7.1: Properties of the tested fuels*

It is visible that n-heptane presents lower viscosity, compared to iso-octane. From the physical definition of viscosity, it represents the resistance to motion opposed by a fluid to the tangential force per unit area. Hence, penetration should be higher for fuels with lower viscosity, as reported in [32].

This would explain why, as indicated in *Figure 7.6*, n-heptane penetrates faster than iso-octane, for both the injection pressures tested. However, variations in fluid properties have little influence on the penetration, comparing these two different kinds of fuels, given that there is not much difference in their properties. For instance, if n-hexane had been used for the tests, we would have expected a major difference in the trends of the plots.

#### **7.1.4 Effect of the temperature chamber variation**

As already visible from the results of section 7.1.1, the back temperature (ambient temperature) plays a decisive role on the length of liquid and vapor penetration, because of the evaporation process. As it can be seen in *Figure 7.7*, the back temperature was varied from 573 K to 800 K. The fuel used was iso-octane, injection pressure fixed at 200 bar, ambient

pressure varied from 3 to 10 bar, to assure the validity of the results for all conditions.

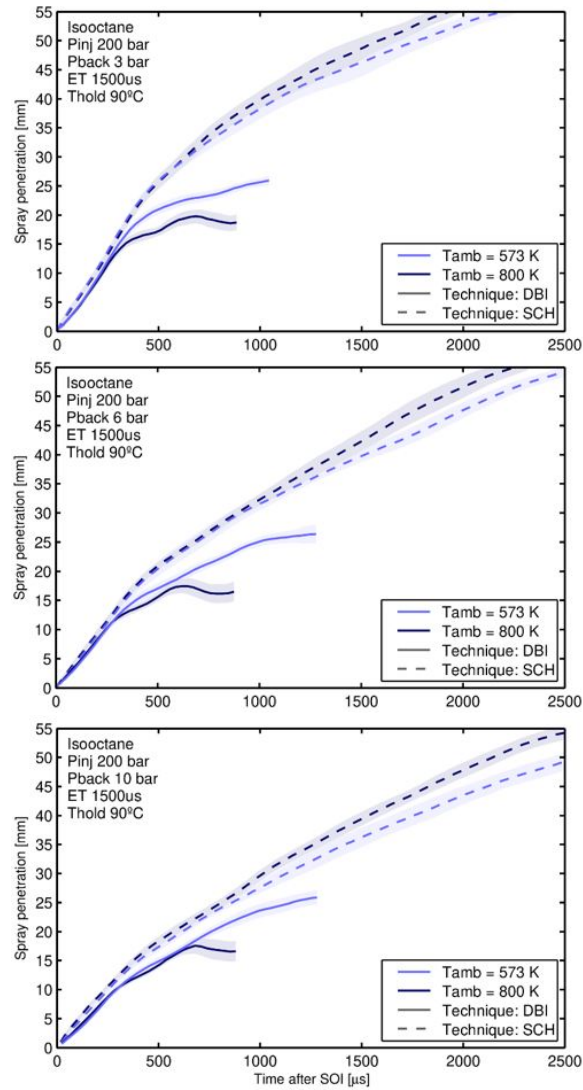


*Figure 7.7: Effect of the back temperature change on liquid and vapor penetration*

In general, it can be argued that, for all the conditions, an increasing in the back temperature to 800 K leads to a decrease in liquid penetration. However, the evaporation process is enhanced with increasing temperature, thus increasing

vapor penetration.

This is the consequence of a faster phase transition of the fuel from liquid to vapor, when the temperature is increased. As it is visible in the graphs, indeed, not only the dark line reaches lower penetrations, but it is also shorter compared to the lighter one. Under higher back temperatures, the liquid phase disappears earlier in time than under the 573 K condition. This is reflected in a larger amount of vapor particles in the chamber, consequently leading to a greater vapor penetration.

## 7.2 Spray angle

The angle measurements are essential to understand and solve the issue of spray collapse, starting by investigating in which conditions it appears. For each time window, the interval considered for the angle fit is from 1% to 50% of the penetration value at that specific time. As in the penetration case, each curve plotted in the graphs is the result of the average of ten measurements repeated under the same condition. Although all the conditions have been tested and processed, just the most significant ones are reported in this paragraph. The others can be found in *Appendices*.

### 7.2.1 Effect of injection pressure variation

Like for the penetration case, three injection pressure level cases (100, 200, 280 bar) have been analysed for all the gas pressure and temperature conditions tested. Herein, just the cases of the iso-octane with energizing time of 1500  $\mu$ s have been reported, given that they are the most significant for the accomplishment of the study.

In *Figure 7.8* can be noted that the angle values of the spray are not very affected by the variation of injection pres-

sure. For the spray angles there is not substantial difference as in the penetration. This happens because, as it will be proved in the following tests, the shape of the spray depends mostly on the conditions of the ambient and not on those of the fluid, with exception of the injection temperature.

In conclusion, the injection pressure has a considerable impact only on the penetration length of the spray, while the angles depend more on the chamber conditions, as it is proved in the following sections.

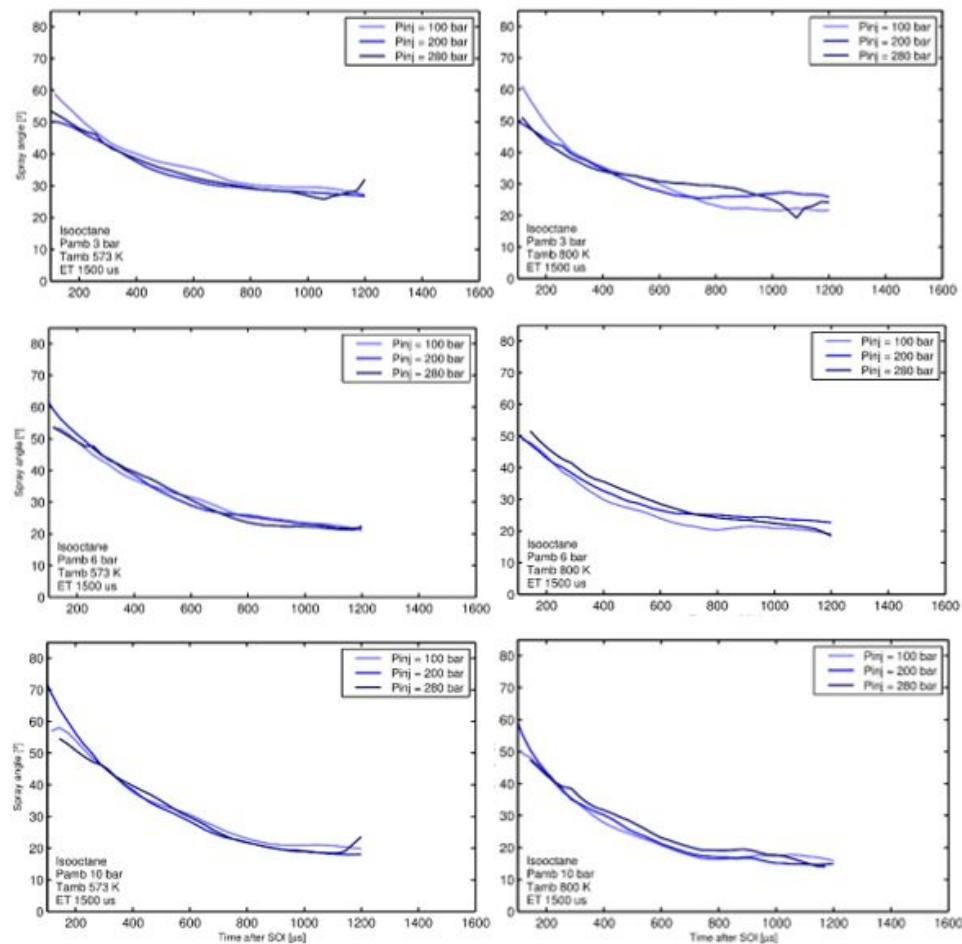


**Figure 7.8:** Effect of the injection pressure on the spray liquid angle

### 7.2.2 Effect of density chamber variation

A wide range of gas-density values may be encountered within a GDI engine and the injector must always supply the proper quantity of fuel at all the possible conditions. As it will be evident by the results, density has a key role for the angle characterisation of the spray, more in terms of spray angle than penetration. As already reported previously, just DBI method has been tested for this characterization as liquid angle is the main parameter which affects the spray collapse phenomenon.

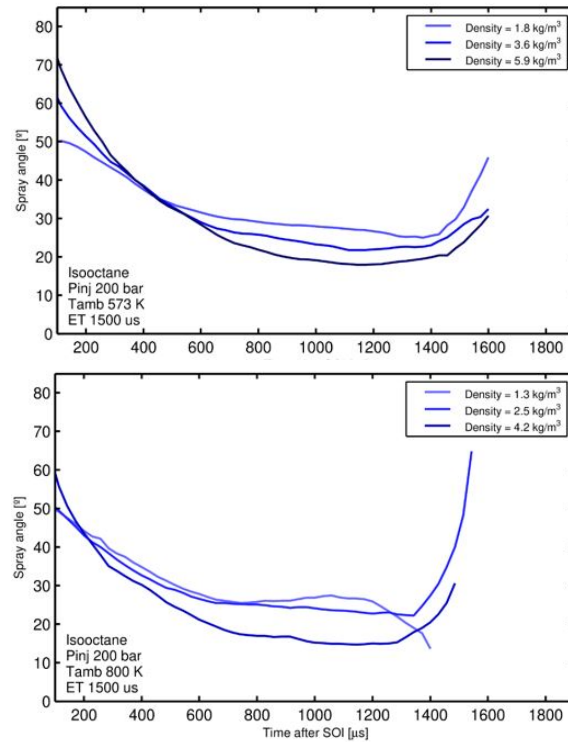


**Figure 7.9:** Effect of back density on spray angles at 573 K (top) and 800 K (bottom)

Figure 7.9 shows liquid spray angle, for different density values, at 573K (top) and 800K (bottom) of chamber temperature with the following test conditions: iso-octane with

injection pressure of 20 bar, energizing time of 1500  $\mu\text{s}$ , fuel exit temperature fixed to 90°C. The major energizing time has been chosen for these results as it means a longer injection time, hence a better visualization of the trend in the graphs.

At a fixed injection pressure and temperature chamber, hence considering the top case at 573 K in *Figure 7.9*, it is evident that a higher value of density is accompanied by a smaller spray angle. Expected trend should be that the more ambient density is increased, bigger spray angles should be detected. Indeed, from the ideal gas law:

$$p_{amb} \sim \rho_{amb} \cdot T_{amb} \quad (7.1)$$

increasing density means a rise in ambient pressure, which leads to an anticipated brake of the spray, with a consequent smaller penetration and bigger angles.

This is true, in this investigation, just for the first part of the injection, namely until about 400  $\mu\text{s}$  ASOI, at 573 K. Afterwards, an inversion of the trend is evident. However, if just one spray plume (and not a spray cone composed by a number of plumes, like in the investigation) was considered,

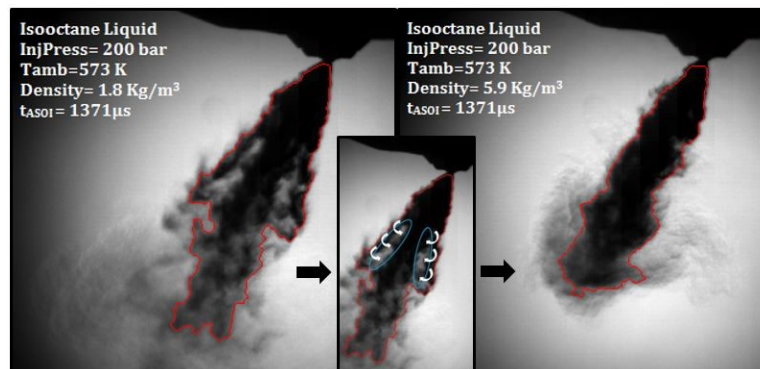


*Figure 7.10: Comparison between raw images at two different density conditions (time ASOI 1371  $\mu\text{s}$ )*

there would not be the inversion and the initial trend would be visible for all the injection. The reason of the inversion is that increasing the ambient density using a multi-hole injector leads to the formation of a low-pressure core between the spray plumes, which will become bigger when the density (and then the cone angle) is increased. The effect of the low-pressure core is that the spray plumes are sucked inward, consequently producing a narrowing of the spray cone. This effect is the so-called spray collapse (*Figure 7.10*).

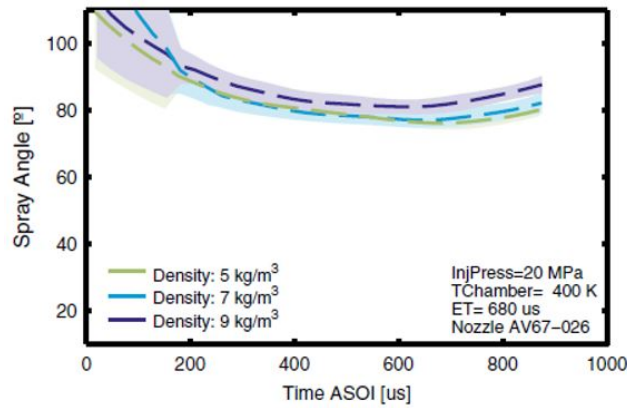


**Figure 7.11:** Density variations at non-vaporizing conditions (400 K) for liquid spray [26]

With the rise in chamber temperature (to 800 K, at the bottom in *Figure 7.9*), it is visible that the inversion of the trend is anticipated at 200  $\mu\text{s}$  ASOI. The reason is that, always bearing in mind the ideal gas law, the effect of density and temperature are combined here, leading to a bigger rise in the pressure. Consequently, this means bigger plume angles and enhanced collapse phenomenon. This trend is highlighted in [26], where same conditions are tested with a very low temperature of 400 K. As it is visible in the graph reported in *Figure 7.11*), the value of temperature is too small for the collapse to occur, given that vaporization cannot oc-

cur at this temperature. Then, higher density values are associated with higher spray angles.

### 7.2.3 Effect of the temperature chamber variation

To assess the effect of ambient gas temperature, only the ambient temperature is varied while holding all other conditions constant. The rapid evaporation typically causes significant distortion of the spray structure, with the in-cylinder flow field now able to easily influence the smaller fuel droplets and in many cases causing individual spray plumes to collapse towards each other, destroying any initial plume directionality initially imparted by the nozzle geometry.

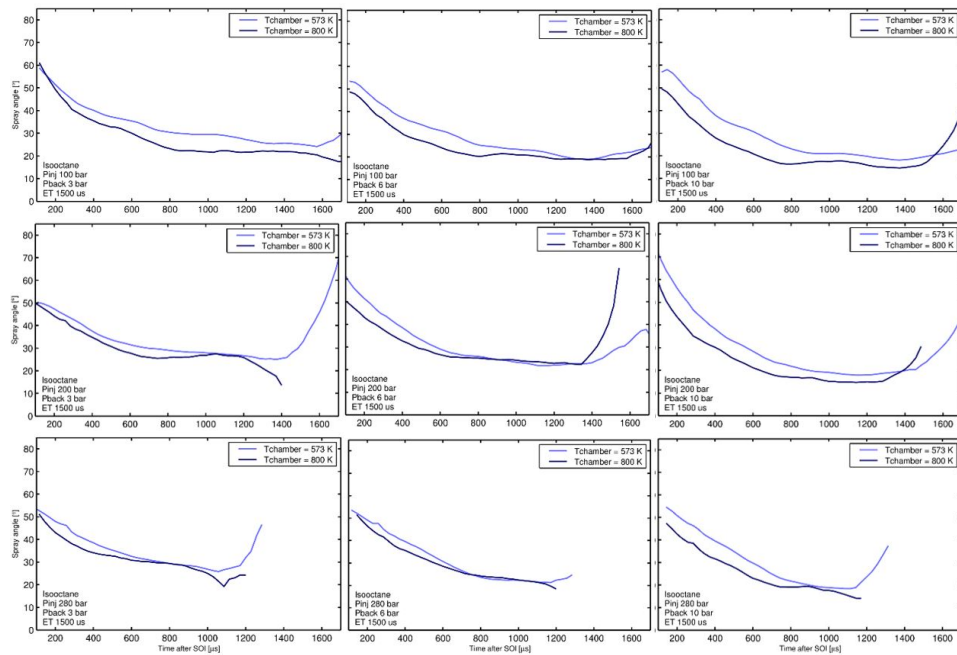


**Figure 7.12:** Effect of the ambient temperature variation on the spray angles

Here in *Figure 7.12*, iso-octane liquid spray with energizing time of  $1500 \mu\text{s}$  are investigated, for all the conditions of injection pressure and background pressure. Temperature

varied between 573 K and 800 K (enhancing the evaporation conditions).

It can be noted that the low temperature curve (573 K) is always positioned above the maximum temperature one. It follows the theory of spray collapse, as previously explained in the section 4.3.2. Anyway, the phenomenon depends also on the other physical factors of the chamber.

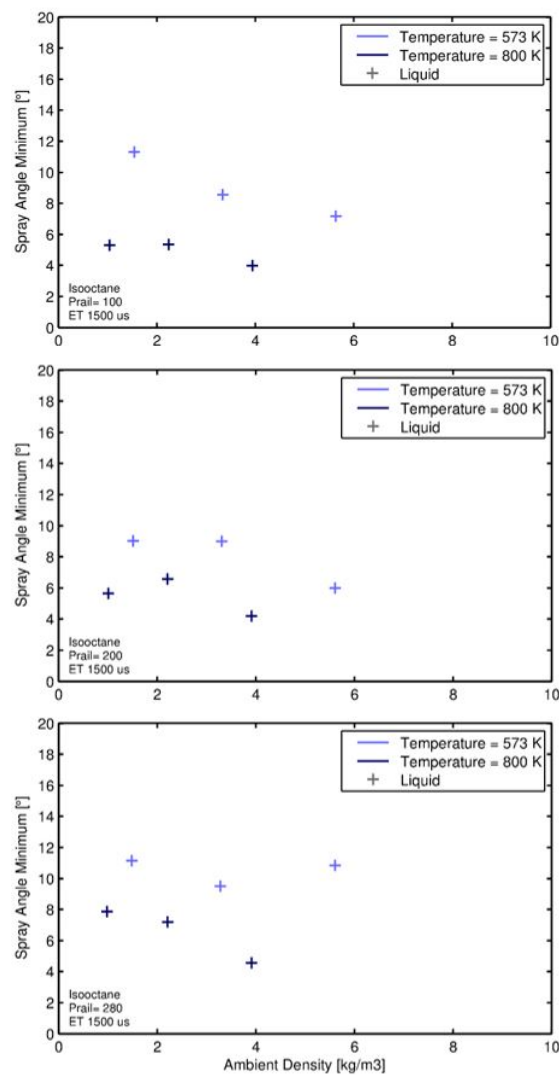


**Figure 7.13:** Combined effects of variations in ambient density and temperature for three injection pressure tested

One possibility to describe the spray collapse process with a single scalar value is to consider the minimum of the spray angle in a certain time window of the injection (800–1500 timeASOI). It should be noted that this analysis is often performed in other studies (mostly in the Diesel spray) by averaging a stabilized zone of spray penetration or spray angle. Nonetheless, in this case, since spray angle do not reach stabilization except for a few of the tested conditions, the minimum of the spray angle in the region near the end of injection was chosen. *Figure 7.13* shows the minimum angle calculated as previously stated for all of the conditions at 100, 200, 280 bar of injection pressure versus the chamber density.

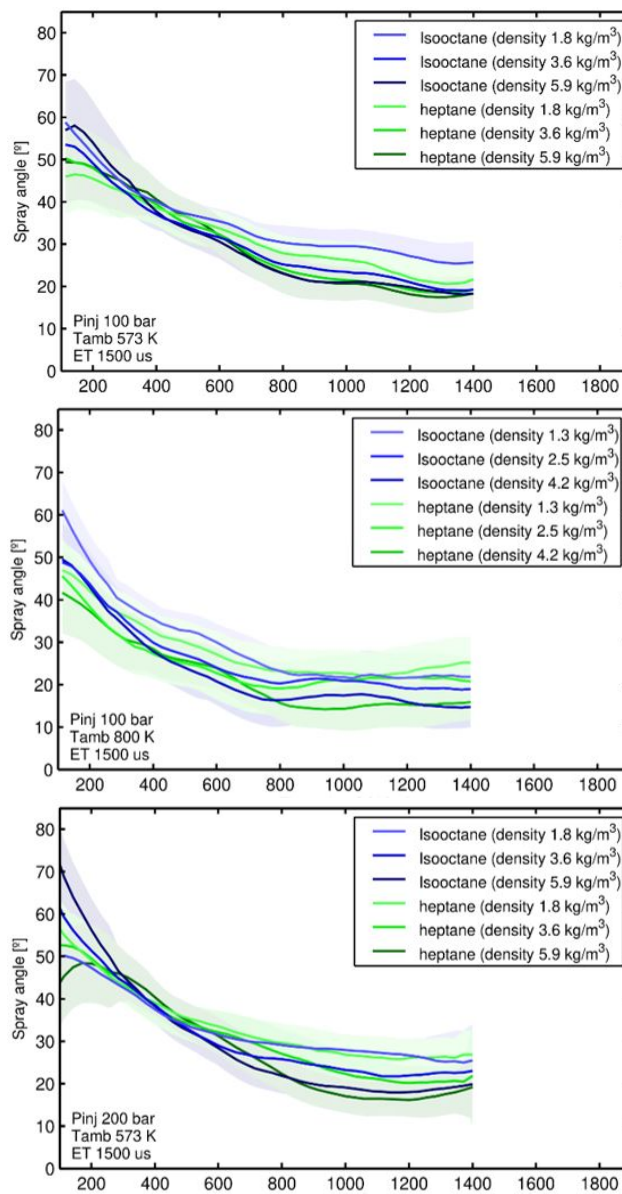
It can be noted that, when either temperature chamber or ambient density are increased, the minimum angle value becomes smaller. Indeed, considering the highest value of ambient density at the highest value of temperature chamber, for all the three cases of injection pressure, the minimum value of the minimum spray angle can be found. This result makes sense in view of previously presented results which reflected that the spray collapse intensifies the higher the chamber temperature and density become.

#### **7.2.4 Effect of the fuel type**

In this section, the results of the tests with both iso-octane and n-heptane are analysed, in order to assess the effect of fuel properties on the spray angles. DBI imaging is used to capture the morphology of the liquid spray cone for the two types of fuel. As before-mentioned, only the liquid spray results are analysed for the angle characterization, given the importance of the liquid volume for the engine performances.

*Figure 7.14* shows the trends of the spray angles for each of the two fuels tested. Ambient densities of the chamber

are varied in each graph, for all the combinations of injection fuel and temperature chamber tested. The results shown are for energizing time of  $1500 \mu\text{s}$ , for the same aforementioned reason. It is visible that the two fuels follow the same trend, thereabouts. The reason for that lies in the combined effect of two parameters of the fuel, which balance each other out: volatility and viscosity.



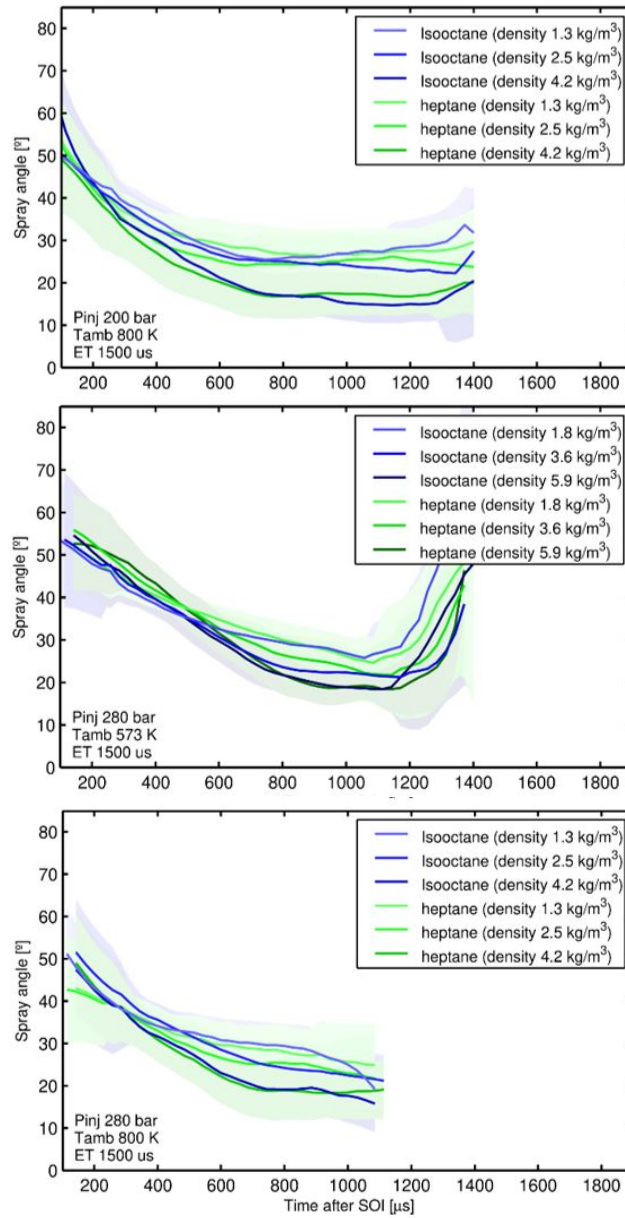


**Figure 7.14:** Comparison of different kinds of fuel under several conditions

Heptane is more volatile than iso-octane (*Figure 7.15*), hence the rate of evaporation is greater. For this reason, also considering the raw images of *Figure 7.16*, it is clear that the contour of the spray is more linear and homogeneous for iso-octane, while it is a lot more non-uniform for heptane. This happens because the rate of evaporation greater leads to major tangential shifts, increasing the cone angle. For this particular situation the raw images are a lot more significant than the graphs in this situation.

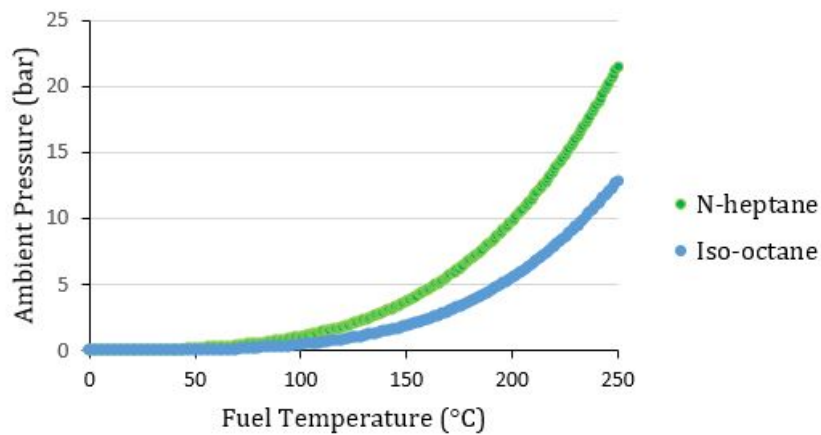


*Figure 7.15: Saturation curve of tested fuels*

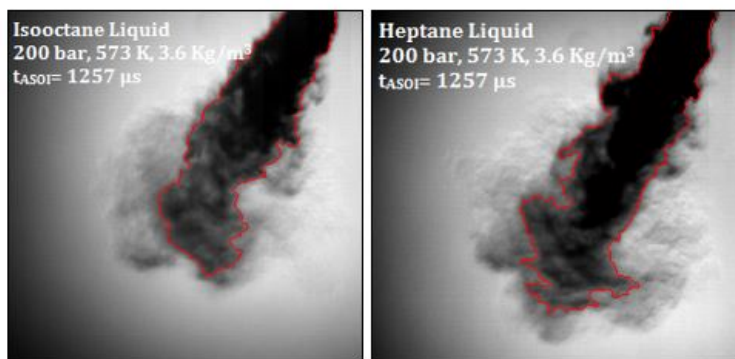


*Figure 7.16: Comparison of raw images: iso-octane (left) and n-heptane (right)*

At the same time, the viscosity of heptane is lower, leading to a greater penetration (as seen in the chapter 7.1.3), hence reducing the size of the cone angle. The combination of these two effects leads to the final conclusion that variations in fluid properties have little influence on the radial penetration, since this is virtually identical for the fuels studied.

### 7.2.5 Effect of the injection temperature variation

The only parameter not investigated in the present work but nevertheless very important for the characterization of the spray is the fuel injection temperature. It has not been investigated due to the vast knowledge provided in literature.

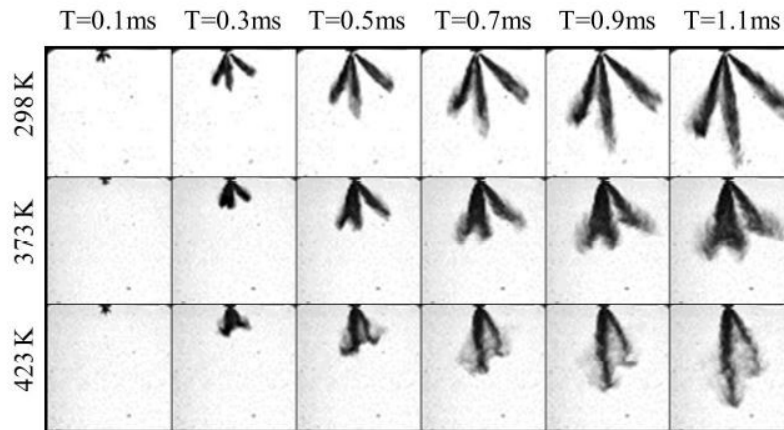


*Figure 7.17: Spray morphology of iso-octane at three different fuel temperatures [33]*

In the present work, indeed, the value of injection temperature is fixed at 90 °C for all the tests. However, for the sake of completeness, many observations on the injection temperature variation made as part of other studies are reported [33]. Increasing fuel temperature, it has been found that all the fuels show significant change in spray morphology due to the changing of the flash boiling degree, as it is clear in

*Figure 7.9.* In macroscopic parameters, as fuel temperature is increased, major observations are reduction in spray cone angle and increase in spray penetration length, due to the enhanced collapse phenomenon caused by flash boiling conditions.

## Chapter 8

# Summary and Conclusions

In this study, the spray characteristics of a six-hole gasoline direct injector were investigated, using high-speed imaging, in a constant volume vessel, at different ambient pressures and back temperatures: the ambient pressure ranged from 3 bar to 21 bar and the ambient temperatures varied from 573 K to 800 K. The fuel temperature fixed at 90 °C, while injection pressure set at 100, 200, 280 bar. Two kinds of fuels have been investigated: iso-octane and n-heptane. For each condition, 10 measurements have been tested and the average of them plotted in graphs to draw conclusions.

In general, results obtained from the penetration are useful to avoid impingement of the fuel on the piston head and cylinder walls, while results from spray angle are worthwhile to investigate in which conditions the collapse phenomenon may appear.

The results obtained through the investigation on liquid and vapor penetration of the spray have indicated the effects listed below.

1. Both liquid and vapor penetration decrease as the ambient pressure or density increases due to the major air resistance encountered by the particles exiting from the nozzle.

2. Injection pressure of the fuel is not a very influent parameter on the liquid penetration, while vapor penetration increases under increased injection pressure. Indeed, under higher pressure of the fuel, the evaporation phenomenon is enhanced.
3. Comparing different kinds of fuel, n-heptane presents greater penetration than iso-octane ones, due to its lower viscosity. Nevertheless, the difference is not considerable because there is not too much gap in their dynamic viscosity.
4. Raising the ambient temperature results in a liquid penetration decrease and vapor penetration increase. This trend is verified for all the temperatures below the threshold after which the flash boiling process starts.

In the characterization of the spray angles, attention is given to the spray collapse phenomenon. Collapses were observed and analysed in several thermodynamic conditions. The main conclusions are as follows.

5. As regards the variation of fuel conditions, there is substantial difference between the effects caused by pressure and temperature. It is proved that injection pressure has not considerable impact on the spray angle. The shape of the spray, on the contrary, significantly depends on the injection temperature: from other works in the literature, it is proved that increasing fuel temperature leads to a reduction of the angle and to increased penetration, due to the collapse caused by the flash boiling.
6. Concerning the variation of chamber conditions, the relations between penetration and angle with density and temperature are presented and it is stated that spray collapse requires both parameters to be moderate or high

to develop. Indeed, it is evident that a rise in whether density or temperature is followed by a weakened radial expansion of the jet.

7. Variations in the type of fuel used have little influence on the spray angle because of the combined effect of its properties. N-heptane, compared to iso-octane, presents lower viscosity and greater volatility, entailing respectively intensified penetration (and so, reduced angle) and increased radial penetration. Obviously, the result is that a change in the fuel used affects more the penetration than the angle of the jet.

Therefore, it is hypothesized that spray collapse is likely a phenomenon caused by whether high density and temperature of the chamber or flash boiling conditions. In the thesis is investigated and analysed the first one, named jet-induced collapse, result of the air entrainment that creates low pressure zones in the centre of the spray plume pulling the spray inwards. This leads disadvantages because the jet suffers a reduction in its volume, losing energy for the following combustion.

It should be noted that the conclusions may only be suitable for the injectors with similar hole configuration to this one but the theory behind it is applicable for other configurations subjected to the same thermodynamic conditions described above.

Nonetheless, lack of knowledge in the literature concerning the condensation-induced spray collapse is still a big issue to solve, for a better understanding on the causes, the conditions in which it occurs and the effects it leads. Thus, the investigation on flash boiling conditions leading to condensation-induced collapse phenomenon represents a possible way to continue the work presented in this thesis.

# Bibliography

- [1] Belgium, B. (2017). *Review of EU-Third Country Cooperation on Policies Falling within the ITRE Domain in Relation to Brexit*. <http://www.europarl.europa.eu>
- [2] *Explaining road transport emissions*, © EEA, Copenhagen, 2016.
- [3] EEA. (2016). *Explaining road transport emissions. A non-technical guide*. European Environment Agency. <https://doi.org/10.2800/71804>
- [4] Hartmann, G. (2007) *Les moteurs et aeroplanes Antoinette*. Available from: <http://www.hydroretro.net/etudegh/antoinette.pdf>
- [5] Bahattin, Mustafa and Ozdaly, Bulent. *Gasoline Direct Injection*. "Fuel Injection". Ed. By Daniela Siano. Chapter 1. Sciyo, 2010
- [6] Seoksu Moon, Essam Abo-Serie, Choongsik Bae. *The spray characteristics of a pressure-swirl injector with various exit plane tilts*. "Fuel Injection". Elsevier, 2008
- [7] Cheng, P., Li, Q., Chen, H., Kang, Z. (2018). *Study on the dynamic response of a pressure swirl injector to ramp variation of mass flow rate*. Acta Astronautica. <https://doi.org/10.1016/j.actaastro.2018.08.049>

- [8] Florian Zentgraf, Elias Baum, Benjamin Böhm, Andreas Dreizler, Brian Peterson. *Analysis of the turbulent in-cylinder flow in an IC engine using tomographic and planar PIV measurements*. 7th International Symposium on Applications of Laser Techniques to Fluid Mechanics Lisbon, Portugal, 07-10 July 2014
- [9] Konstantinoff, L., Pfeifer, C., Pillei, M., Trattnig, U., Dornauer, T., Möltner, L. (2017). *Optimization of the Charge Motion in Sewage Gas - Driven Internal Combustion Engines for Combined Heat and Power Units*. 11, 82–91
- [10] Kim, Nouri, Yan, Arcoumanis. *Effects of intake swirl and coolant temperature on spray structure of a high-pressure multi-hole injector in a direct-injection gasoline engine*. Third International Conference on Optical and Laser Diagnostics. 2007
- [11] Mahklouf, Hélie, Grimoux, Gestri, Cousin, Wood, Wigley. *Spray resulting from High Pressure Atomization with low  $L$  over  $D$  Multihole injectors and the role of the cavitation*. 12th International Conference on Liquid Atomization and Spray Systems. Heidelberg, 2012
- [12] Lefebvre, A. (1989). *Atomisation and Sprays*. Taylor and Francis
- [13] Rink, Lefebvre. *Influence of Fuel Drop Size and Combustor Operating Conditions on Pollutant Emissions*. SAE, 1986: SAE Paper 861541
- [14] Zhao, Harrington and Lai. *Automotive gasoline direct injection engines*. SAE International, 1999

- [15] Ohnesorge. *Formation of drops by nozzles and the breakup of liquid jets*. Journal of Applied Mathematics and Mechanics, 1936: Vol.16 p.355-358
- [16] Rayleigh. *On the instability of jets*. Proceedings of the London Mathematical Society, 1878: Vol.10 p.4-13
- [17] Reitz. *Atomization and other Breakup Regimes of a Liquid Jet*. Princeton University: PhD Thesis, 1978
- [18] Park, Yoon, Lee. *Effects of multiple-injection strategies on overall spray behavior, combustion, and emissions reduction characteristics of biodiesel fuel*. Applied Energy, 2011: Vol.88 p.88-98
- [19] Abart, Schmidt, Schoegl, Trattner, Kirchberger, Eichlseder and Jajcevic. *Basic Investigations on the Prediction of Spray-Wall and Spray-Fluid Interaction for a GDI Combustion Process*. SAE, 2010: SAE Paper 2010-32-0030
- [20] Wang, Z., Li, Y., Guo, H., Wang, C., Xu, H. (2018). *Microscopic and macroscopic characterization of spray impingement under flash boiling conditions with the application of split injection strategy*. "Fuel", 212(October 2017), 315–325
- [21] Li, Y., Guo, H., Ma, X., Qi, Y., Wang, Z., Xu, H., Shuai, S. (2018). *Morphology analysis on multi-jet flash-boiling sprays under wide ambient pressures*. "Fuel", 211(April 2017), 38–47. <https://doi.org/10.1016/j.fuel.2017.08.082>
- [22] Park, Lee. *An Experimental Investigation of the Flash Atomization Mechanism*. "Atomization and Sprays", 1994: 159-179
- [23] Mojtabi, M., Chadwick, N., Wigley, G., Helie, J. (2008). *The effect of flash boiling on break up and*

- atomization in GDI sprays*. 22nd European Conference on Liquid Atomization and Spray Systems, 8–10. <https://doi.org/ILASS08-6-1>
- [24] Kawano, Goto, Odaka, Senda. *Modelling Atomization and Vaporization Processes of Flash Boiling Spray*. SAE, 2004: SAE Paper 2004-01-0534
- [25] Guo, H., Ding, H., Li, Y., Ma, X., Wang, Z., Xu, H., Wang, J. (2017). *Comparison of spray collapses at elevated ambient pressure and flash boiling conditions using multi-hole gasoline direct injector*. "Fuel", 199, 125–134. <https://doi.org/10.1016/j.fuel.2017.02.071>
- [26] Payri, R., Salvador, F. J., Martí-Aldaraví, P., Vaquerizo, D. (2017). *ECN Spray G external spray visualization and spray collapse description through penetration and morphology analysis*. Applied Thermal Engineering, 112, 304–316. <https://doi.org/10.1016/j.applthermaleng.2016.10.023>
- [27] Eduardo Abad Camarero. (2019). *Implementación de un sistema térmico para la realización de ensayos de inyección directa de gasolina*. Universidad Politécnica de Madrid, 5–10
- [28] Davidhazy, A. (2006). *Introduction to shadowgraph and schlieren imaging*. Recommended Citation. <http://scholarworks.rit.edu/article/478>
- [29] Mazumdar, A. (2011). *Principles and Techniques of Schlieren Imaging*. Columbia University, 1–16. <http://hdl.handle.net/10022/AC:P:20839>
- [30] Payri, R., Salvador, F. J., Gimeno, J., Viera, J. P. (2015). *Experimental Analysis on the Influence of Nozzle Geometry Over the Dispersion of Liquid N-Dodecane*

*Sprays*. *Frontiers in Mechanical Engineering*, 1(November). <https://doi.org/10.3389/fmech.2015.00013>

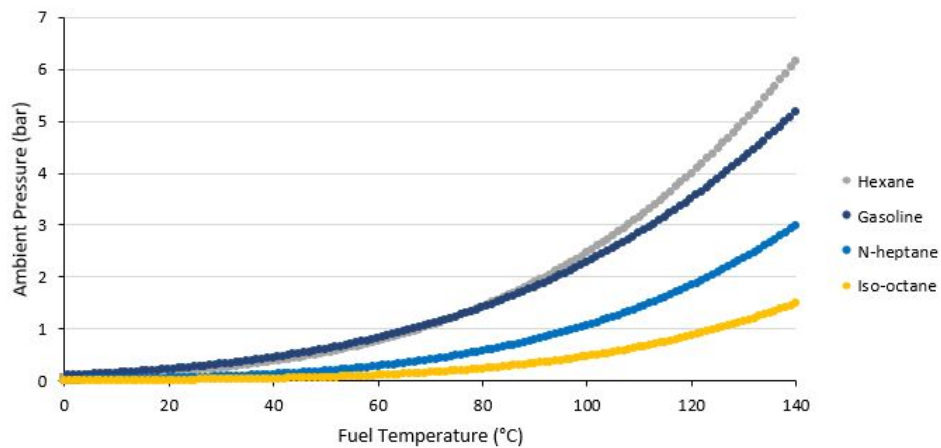
- [31] Tonini, S., Gavaises, M., Arcoumanis, C., Theodorakakos, A. (2006). *Prediction of liquid and vapor penetration of high-pressure diesel sprays*. SAE Technical Papers, April. <https://doi.org/10.4271/2006-01-0242>
- [32] Wigley, G., Mehdi, M., Williams, M., Pitcher, G., Hele, J. (2006). *The effect of fuel properties on liquid breakup and atomisation in GDI sprays*. 10th International Conference on Liquid Atomization and Spray Systems, ICLASS 2006, (January)
- [33] Vincent, T. L., Green, P. J., Woolfson, D. N. (2011). *Optical investigation of flash boiling and its effect on in-cylinder combustion for butanol isomers and iso-octane* (Vol. 0, pp. 4–11).

# Appendices

*Principal proprieties of the material used for the realization of the test rig*

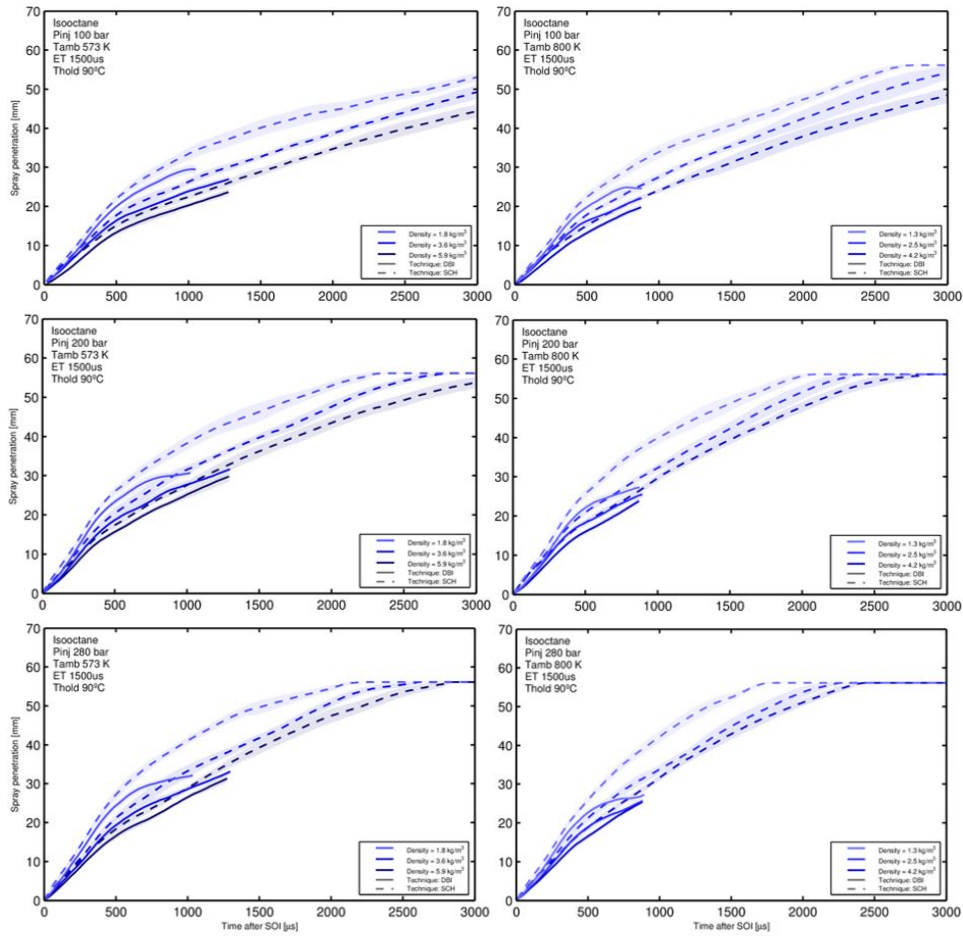
<b>Material</b>	<b>AISI 1020 steel, cold rolled</b>
Density (Kg/m <sup>3</sup> )	7870
specific heat (J/Kg K)	480
heat conductivity (W/m K)	51.9

*Saturation pressure of a real commercial European gasoline compared to other components*



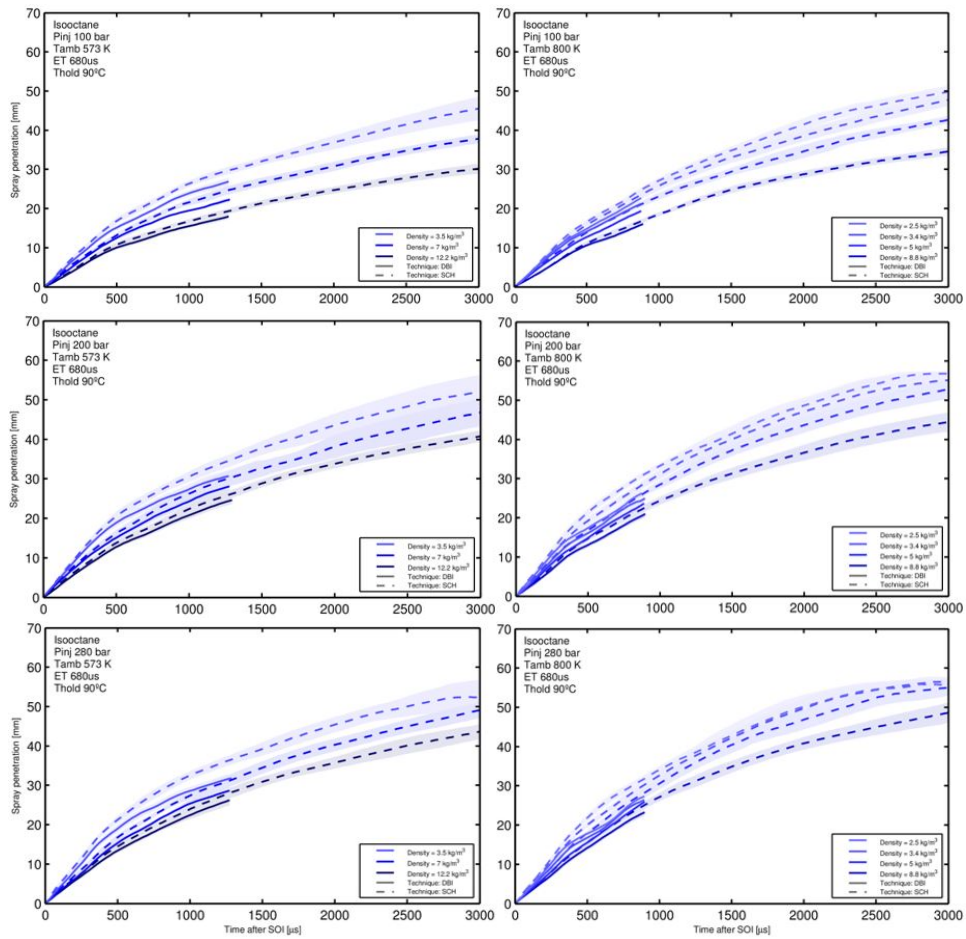
## Iso-octane, penetration vs ambient density

- ET 1500



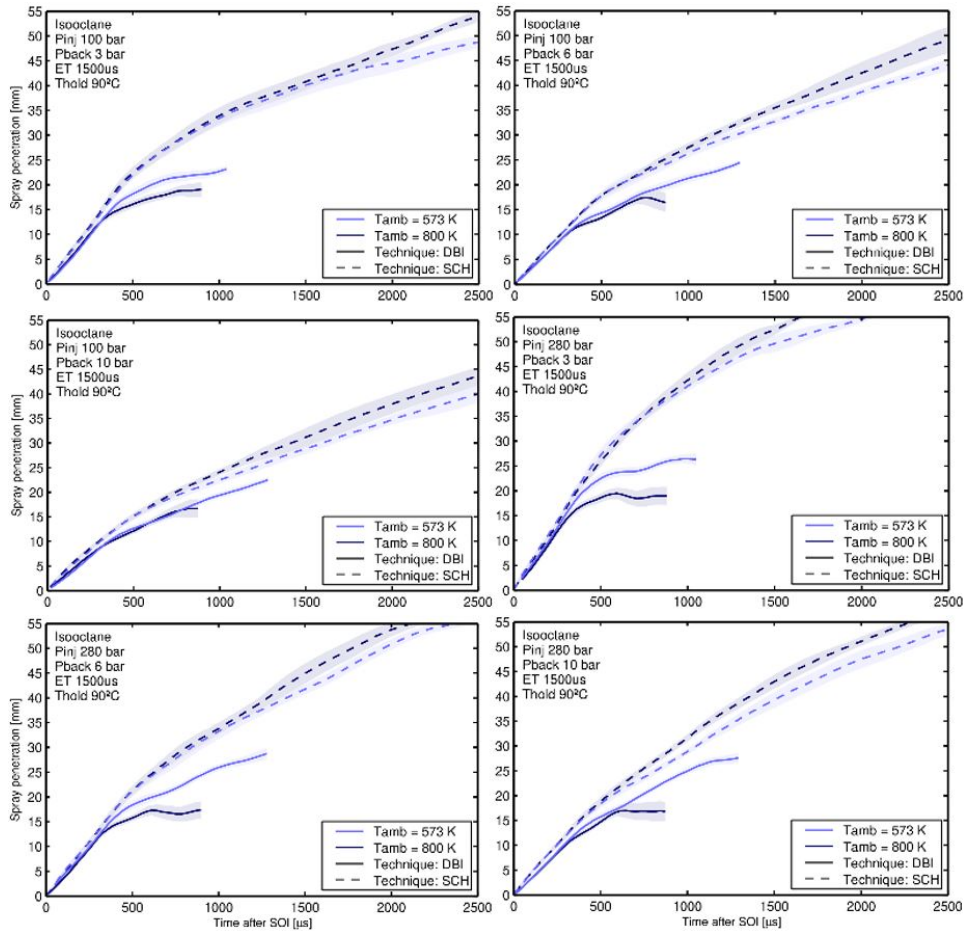
## Iso-octane, penetration vs ambient density

- ET 680



*Iso-octane, penetration vs ambient temperature:*

- *ET 1500*



*Iso-octane, penetration vs ambient temperature:*

- *ET 680*

